國立臺灣大學牙醫專業學院口腔生物科學研究所

碩士論文

Graduate Institute of Oral Biology College of Dentistry

National Taiwan University

Master Thesis

活細胞分析式微流道晶片之開發及其應用於癌症轉移潛能診斷之評估

暨

SIK2 藉由磷酸化 CAPS2 調控胰島素分泌之探討

Study I: A portable microfluidic device for the rapid diagnosis of cancer metastatic potential

Study II: Identification of CAPS2 as a downstream target of SIK2 in regulating insulin secretion

陳立瑜 (Li-Yu Chen)

指導教授：周涵怡 博士 (Han-Yi Chou, Ph.D)

中華民國 104 年 7 月

July, 2015

研究一 活細胞分析式微流道晶片之開發及其應用於癌症轉移潛能診斷之評估

摘要

肺癌的轉移若及早發現並加以治療，便能顯著提升患者改善病情的機會。然而，現行臨床癌症檢驗之方式，如胸腔攝影、斷層掃描及組織切片等，均未能有效判斷肺癌細胞轉移之可能性，以致患者無法獲得適當的治療。本研究中，吾人設計開發出一新型微流道晶片系統，以期作為快速評估癌症轉移潛能之臨床檢驗。本系統設計係以恆定環境溫度及酸鹼度為基礎，再以甲殼素附著之微流道表面偵測目標細胞之貼附性，作為判斷細胞遷移特性之依據。於實際測試中，吾人將不同轉移潛能之肺癌細胞株，經標定後以本系統進行細胞貼附性測試。結果顯示本系統確能有效區分不同轉移潛能之肺癌細胞株。因此，透過本系本研究所開發之微流道系統，僅需少量自患者經活體採樣分離之細胞樣本，便能迅速取得評估癌細胞轉移潛能之資訊。此微流道系統未來若能應用於臨床診斷，便能為肺癌及其他癌症患者，於早期研判適合之治療模式。

Study I: A portable microfluidic device for the rapid diagnosis of cancer metastatic potential which is programmable for temperature and CO_2

Abstract

If metastasis of lung cancer can be found and treated early, a patient might have an improved chance to prevail over it, but routine examinations such as chest radiography, computed tomography and biopsy cannot characterize the metastatic potential of lung cancer cells; critical diagnoses to define optimal therapeutic strategies are thus lost. In this study, we designed a portable microfluidic device for the rapid diagnosis of cancer metastatic potential. Featuring a micro system to control temperature and a bicarbonate buffered environment, our device discriminates a rate of surface detachment as an index of the migratory ability of cells cultured on pH-responsive chitosan. We labeled metastatic subpopulations of lung cancer cell lines, and verified that our device is capable of separating cells according to their metastatic ability. As only few cells are needed, a patient's specimen from biopsies, e.g. from fine-needle aspiration, can be processed on site to offer immediate information to physicians. We expect that our design will provide valuable information in pre-operative evaluations to assist the definition of therapeutic plans for lung cancer, as well as for metastatic tumors of other types.

Background

Lung cancer, the foremost cause of cancer related deaths

Nowadays, the biggest challenge in medical is cancer, the leading cause of death worldwide, accounting for 8.2 million deaths in 2012. Around 90% of all cancer deaths are the result of metastases, the spread of cancer from its primary site to other places in the body, rather than of the primary tumors [1].

Among plenty of cancers, lung cancer is the most usually diagnosed malignancy in the world. Meanwhile, lung cancer is the foremost cause of cancer mortality worldwide, accounting for 1.3 million deaths annually and the 5 year survival rate is only about 15% [2]. It is common among men in terms of both incidence and mortality, and among women has the third highest incidence, and is second after breast cancer in mortality [3]. In approximately 40% of patients diagnosed with lung cancer, the diagnosis is made after the disease has advanced because lung cancer may not produce any noticeable symptoms in the early stages. Those early metastasized lung cancers could not be detected before they have become aggravated, causing bad prognosis with a high mortality rate. The only way to decrease mortality of lung cancer patients is to detect it, diagnose it and treat it as early as possible.

Routine examinations for lung cancer and its limitations

Approximately 85% of patients with lung cancer seek medical advice with symptoms, and the remainder is detected by chest radiographic evaluation initiated for other reasons such as general physical examination. Routine diagnostic examinations for patients suspected with lung cancer includes imaging test, sputum cytology test and tissue biopsy test (http://www.cancer.org). Chest x-ray is the most common imaging test for screening any abnormal masses or nodules on the lungs, and may sometimes be combined with CT scans to reveal smaller lesions that would not be detected on an X-ray for detailed information. If patients cough and produce sputum, sputum cytology test sometimes help them in finding the presence of cancerous cells. Biopsy test is the remove of suspicious cancer tissues or cells for histological, cytological, or molecular analysis by bronchoscopy passed down from throat and into lungs or by image guided needle through chest wall and into the lung [4]. Definite diagnosis of suspected lung cancer will not be made until cancer cells are detected in biopsied tissues obtained from suspicious lump found by imaging tests under microscope.

However, most patients have initiated the metastatic process by the time of diagnosis. Although lung cancer is initially detected by imaging morphological changes inside the lungs and confirmed with biopsy tests, unobvious cancer mass or small populations of metastatic cancers cells outside the imaging area are easily missed. In

order to prevent early-staged metastasis before spreading continuously, it is important to understand the metastatic potential of cancer cells and plan treatments referring to this characteristic. To do so, it requires technical challenges to functionally assay live cancer cells from patients' specimens which are accessible from biopsy. Nevertheless, patients' specimens are usually fixed for tissue processing or smear tests rather than cultured because handling of living cells clinically is limited by the consumption of time, costs and manpower. Routine examinations such as histological, cytological, or molecular analysis provide us information about cancer classification, expression of tumor markers or tumor subtyping from biopsied tumor samples instead of direct information on the metastatic potential of cancer. Critical diagnoses to define optimal therapeutic strategies are thus lost.

Aim

To make up for limitations of routine examinations for analyzing metastatic potential of living cell samples, we aim to develop a device which utilizes patients' specimen obtained from biopsy to evaluate metastatic characteristics of cancer cells.

Design

Design Concept

According to our demands, this device was designed based on the following four features. Firstly and fundamentally, it provides a bio-mimic environment such as CO_2 incubator having temperature and pH value controls to keep cells alive. Secondly, it should be small enough to handle very few cells obtained from the fine needle biopsy. Thirdly, it directly perform functional assay of patients' living-cell samples on metastatic characteristics. Fourthly, it can be a portable device offering rapid, on site processing and diagnosing.

Microfluidic chip as a principle part of device

Microfluidic device is also known as a lab-on-a-chip (LOC) device or a micro total analysis systems (μTAS), which integrate and scale down laboratory functions and processes to a miniaturized chip format and shrink all analytic steps to micro-level by manipulating small (10^{-9} – 10^{-18} L) amounts of fluids in channels of micrometer. Currently, microfluidic device has been applied to perform all kinds of biomedical uses because it provides various advantages. For example, volumes of fluids within microfluidic channels are generally in the microliter range, it greatly reduces the use of

reagents and analytes. The reacting turnaround time is shorten as whole analytic processes have been condensed to a chip. In addition, the lower fabrication costs of microfluidic devices allow the production of cost-effective disposable chips. With these properties, microfluidic device is beneficial to deal with restricted amount of samples, and is suitable to be applied as a general diagnostic device. Here we explored the advantages offered by microfluidic device to design a 'Microfluidic Device for Cancer Metastatic Potential', MD-CaMP.

Microfluidic cell culture

On the basis of our aim, live cells from biopsied specimen should be maintained alive from the time being collected out of human body and to the functional analysis. The ability to maintain extracellular environment in a physiological conditions is fundamental for cell culturing. Sometimes when meeting the needs to assay or image live cells for a period of time, most of the laboratory practices utilize microscope incubators to control three important factors – temperature, CO_2 and moisture, to attain proper environments for cells to behave physiologically during experimenting. However, a commercial biological microscope incubator currently takes tens of minutes to reach a steady environment; it is also expensive and energy-consuming.

Development in microfluidics enables us to create tools to control the cellular microenvironment. The possibility of microfluidic device to integrate precise and rapid control of their temperature and CO_2 can be an effective solution [5]. In the case of temperature control, various configurations of a micro-heater have been extensively discussed [6]. For instance, a microfluidic temperature control device for quick and reversible switch of temperature has been used to study the temperature-sensitized microtubule dynamics of cells [7]. Also, the stable carbon dioxide partial pressure on CO_2 chips controlled by the equilibration of pre-equilibrated aqueous flow through the highly gas permeable substrate, poly(dimethylsiloxane) (PDMS) enable long-term culture of mammalian cells. Accordingly, by the incorporation with temperature and CO_2 control, our device MD-CaMP is designed as a minimized cell incubator which provides bio-mimic environment for live cell assaying [8].

Metastatic index

Metastasis is a complex process that involves the spread of cancer to distant parts of the body from its original site. There are several steps of metastasis. At first, cancer cells separate from the primary tumor and Invade through around tissues and their basement membranes. Next they penetrate blood or lymphatics vessels and spread into

circulation. Finally they extravasate and colonize the distant area.

The complicated interactions between tumor cells and the extracellular matrix (ECM) play important roles during tumor metastasis. Abnormal extracellular matrix remodeling is related to metastatic disease and promotes cancer progression [9, 10]. Fibronectin, an extracellular matrix glycoprotein, has been reported to be up-regulated in advanced stage lung cancer cells, and the metastatic potential of lung cancer is positively correlated to the amount of fibronectin expression [11, 12]. Higher production of fibronectin is not only a hallmark of cancer cell mesenchymal epithelial transition, it can also relay intracellular signaling pathways that lead to increased aggressiveness, and is an important factor for the "seed and soil" process for distant lung cancer metastasis [13]. Thus, fibronectin can be considered as an index for assaying lung cancer metastatic potential.

Analytic platform

Since fibronectin is a negatively-charged glycoprotein, we attempted to use a biocompatible and electro positive material as an analytic platform to separate cancer cells with different level of fibronectin by electro affinity. Chitosan, is one of many interesting material fitting our requirement. Produced commercially

by de-acetylation of chitin, the structural element in the exoskeleton of crustaceans, chitosan is well-known in biomedical uses due to the characteristics of biodegradable, biocompatible, bio-adhesive, nontoxic, non-antigenic. Structurally, chitosan is a cationic polysaccharide with a variable number of randomly located N-glucosamine and N-acetyl-glucosamine groups. The protonation–deprotonation equilibrium of the primary amine on its glucosamine residues make it a pH-responsive polycation. The isoelectric point (pI) of chitosan occurs at pH7.4 [14], meaning chitosan carries no electrical charge at pH7.4. In other words, if environmental pH value is lower than its pI, chitosan will be positively charged, and conversely if environmental pH value is greater than its pI, chitosan will be negatively charged. It has been reported that by altering its adsorption to fibronectin, chitosan is capable of controlling cell attachment by adjustment of medium pH [15]. While increasing medium pH (to pH 7.65), over 90% of cells would rapidly detached from chitosan surface within 1 h. Coated as a thin film on the surface of tissue culture dish, chitosan can be a pH-responsive substrate to harvest cells without enzymatic treatments (Appendix 1). Furthermore, mixed cells can be fractionated according to their distinguishing detachment capabilities on chitosan surface [16]. Accordingly, chitosan is applicable as an analytic platform of MD-CaMP for fractionating cancer cells by its affinity to fibronectin.

In this study, we propose the design of a microfluidic device for cancer metastatic potential, MD-CaMP, which enables bedside fractionation of minute mass specimens. MD-CaMP features programmable modules for temperature control, bicarbonate-dependent pH regulation, and a pH-responsive chitosan coating to discriminate the cancer metastatic potential through the adsorption of fibronectin.

Materials and methods

Microfluidic fabrication

The design and fabrication of microfluidic device was made cooperatively with Y. H. Yu and I. F. Yu, department of Mechanical Engineering, College of Engineering, National Taiwan University.

The microfluidic chambers were fabricated on poly(dimethylsiloxane) (PDMS) using soft lithographic methods. The master mould was fabricated on a polymethylmethacrylate (PMMA) plate using a computer numerical control (CNC) machine (EGX-400, Roland Inc., Japan) equipped with a 0.5 mm drill bit at a feeding speed of 7 mm. s^{-1} and a rotational rate of 26,000 rpm. PDMS containing the prepolymer and the curing agent at the mass ratio of 10 : 1 was mixed, degassed in vacuum, poured into the PMMA mould and cured at 80 °C. The PDMS structure was treated with an oxygen plasma before bonding and assembly.

A grid of platinum micro-heaters is fabricated on glass to precisely and rapidly control the temperature based on the feedback signal of a designed micro thermal sensor and a control program. The grid-type micro-heater and micro thermal sensor were fabricated by standard lithography and lift-off. The bio-compatible soda-lime glass (thickness 0.7 mm) was first cleaned with piranha solution (H_2SO_4:H_2O_2 = 3 : 1). A

positive photoresist (AZ 4620, Clariant Inc., USA) was then spin-coated (3000 rpm, 40 s) and patterned with photolithography to define the micro-heaters and the micro thermal temperature sensor. With E-beam evaporation, we deposited a Pt layer (120 nm) above a Cr layer (30 nm) on the glass substrate (0.7 mm). The Pt layer was then patterned with a standard lift-off process to obtain the micro-heaters and the microthermal sensor.

Chitosan preparation and coating

A chitosan substrate was prepared from 0.5％(w/w) chitosan solution dissolved in 3％(w/v) acetic acid [15]. Chitosan substrate was added (30 μL) into the microchannels or (100 μl/cm^2 surface area) into culture dish and dried at 60°C for one day to form a thin film. Then the coating surface needs to be neutralized was by 0.5N $NaOH_{(aq)}$ for 2 hours at room temperature and washed with ddH_2O and 1×PBS once. Before cell seeding, these microchannels and culture dishes were exposed to ultraviolet light overnight and washed thoroughly with PBS again.

Cell Culture

CL1-0, CL1-1 and CL1-5 cells were maintained in RPMI 1640 medium

(Invitrogen) supplemented with 10% fetal bovine serum at 37°C in a 5% CO_2 humidified atmosphere and passage by cell detachment buffer (10 mM EDTA in PBS).

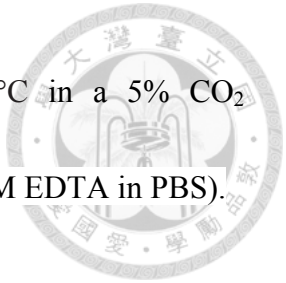

Cell migration and proliferation measurement

For cell migration measurement, wound-healing assay which mimics cell migration during wound healing in vivo was performed.CL1-0, CL1-1 and CL1-5 cells were seeded at same density in 6 well plates until confluent. Making a straight scratch on cultured cells by using a (yellow) pipette tip to create uniform cell-free spaces allows cells to migrate into and "heal" the "wound". Live cell images were captures 24 hours by time lapse microscopy. We measured the original width of the area immediately after the scratch as 100%, and for the subsequent time points, the width were measured again to obtain the remaining percentage of cell-free space.

For cell proliferation measurement, equal amount (1×10^6) of CL1-0, CL1-1 and CL1-5 cells were seeded in 6 well plates and trypsinazed to count the number of cells after culturing for 24 hours by hemocytometer.

Fluorescenct reagent and staining

MitoTracker Red CM-H_2XRos (Invitrogen, M7513), MitoTracker Green FM

(Invitrogen, M7514), Vybrant CFDA SE Cell Tracer (Invitrogen, V12883), Hoechst 34580 (Invrogen, H21486)

For MitoTracker Red CM-H_2XRos and MitoTracker Green FM, dilute 1 mM MitoTrackerstock solution to the final working concentration (25–500 nM) in incomplete medium. When cells have reached the desired confluency, media was removed from the dish, then prewarmed (37°C) staining solution containing MitoTracker probe was added and incubate for 15–45 minutes at 37°C. After staining is complete, the staining solution could be replaced with fresh prewarmed media.

For Vybrant CFDA SE Cell Tracer, dilute the 10 mM stock solution in PBS to working concentration (0.5–25 μM). When cells have reached the desired confluency, media was removed from the dish, then prewarmed (37°C) PBS containing Vybrant CFDA probe was added and incubate for 15 minutes at 37°C. After staining is complete, the staining solution could be replaced with fresh prewarmed media and incubate the cultures for another 30 minutes at 37°C.

For Hoechst 34580, dilute the 10 mg/ml stock solution in PBS to working concentration (0.2 to 5 μg/mL). When cells have reached the desired confluency, media was removed from the dish, then prewarmed (37°C) staining solution containing Hoechst 34580 probe was added and incubate for 20–30 minutes at 37°C. After staining is complete, the staining solution could be replaced with fresh prewarmed media.

Cell seeding and detachment assays on MD-CaMP

1×10^5 CL1 cells were seeded onto the chip coated with chitosan and cultured at pH 7.4 for 16 h. In co-culture experiments, CL1-1 cells and CL1-5 were pre-stained with 300 nM MitoTracker Red CM-H_2XRos (red) and 5μM Vybrant CFDA SE Cell Tracer (blue), respectively, for 15 min at 37 °C and mixed in a ratio of 1 : 1 to seed into the microchannel.

For flushing, a micro-flow syringe pump served to continually infuse PBS (pH7.8) so as to mimic the rate of blood flow in arteries (8 mm s^{-1}).

Cell seeding and attachment assays on culture dish

6×10^5 cells were seeded onto the 35 mm TCPS culture dish coated with chitosan and cultured at pH 7.4 for 0, 1, 2, 3, 4 hr. In co-culture experiments, CL1-0, CL1-1, CL1-5 were pre-stained with MitoTracker Green FM, MitoTracker Red CM-H_2XRos and Hoechst 34580 respectively and mixed in a ratio of 1 : 1：1 to seed onto the 35 mm TCPS culture dish coated with and without chitosan and cultured at pH 7.4 for 0, 1, 2, 3, 4 hr. At each point of time, cells were gently washed three times and imaged for calculation of cells still attached on chitosan surface.

Western blot analysis

Whole cell lysates were extracted by lysing cells with RIPA lysis buffer (20mM Tris/HCl, pH 7.4, 0.15M NaCl, 1mM DTT, 1mM EDTA, 1mM EGTA, 5% glycerol, 0.1% Triton X-100, 1X protease inhibitor (Roche) and 1X phosphatase inhibitor (Roche)) at 4 ℃ for 15 min followed by centrifugation at 13000g, 4 ℃ for 15 min. 30-50 μg of the proteins was separated by 8% SDS-PAGE and eletrophorestically transferred to polyvinylidenedifluoride (PVDF) membranes (PALL) at 300 mA, 2 hr. Membranes were probed with anti-fibronectin antibody [IST-9] (ab6328,abcam) and anti-tubulin antibody (GTX11324, GeneTex) at 4 □, O/N. Horseradish peroxidase-conjugated polyclonal goat anti-mouse secondary antibodies were incubated for 1 hour at room temperature. Polypeptide bands were visualized using ECL chemiluminescent substrates (Advansta**)** and LAS-4000 luminescent image analyzer (Fujifilm).

Results

Design of MD-CaMP

MD-CaMP is designed as a minimized cell incubator which provides a bio-mimic environments — a controlled temperature and partial pressure of CO_2 for live cell analysis without the requirement of a general cell-culture incubator.

This device contains two parts; the micro-temperature control system and the main body of this device, microfluidic chip (Figure 1A). Micro-temperature control system, including a micro-heater and a micro thermal sensor, stably provides physiological temperature maintenance at 37°C (Figure 1C). Functionally, the micro-temperature control system was placed underneath the microfluidic chip and controlled temperature from the bottom of the device (Figure 1E). And the main body of this device, microfluidic chip, is composed of outer CO_2 chambers and inner cell culture chambers (Figure 1B, D). The outer CO_2 chamber is a bicarbonate buffered environment filled with $NaHCO_3$ solution for the adjustment of medium pH value through CO_2 penetrating a gas-permeable PDMS wall of chamber ; the inner chamber is a cell culture area with chitosan coated surface on which cancer cells are assayed for their metastatic potential. In addition, the optically clear microfluidic chip made by PDMS permits direct cell observation under microscope. We hope MD-CaMP design

can help to fractionate biopsy or operative samples to provide a rapid index of the cancer metastatic potential.

Migratory abilities of CL1-0, CL1-1 and CL1-5 Cell model for MD-CaMP testing

After the design and fabrication of MD-CaMP, we started to test its function and feasibility. For testing model, we choose three human lung adenocarcinoma sublines CL1-0, CL1-1 and CL1-5, which are subpopulations from a clonal cell line CL1. CL1 was established from a human subject (age 64 years) with a poorly differentiated adenocarcinoma. Subpopulations (sublines CL1-0, CL1-1 and CL1-5) from CL1 cells were selected according to their differing invasiveness through a Boyden chamber, and sibling cell clones were assigned according to the number of rounds through a Boyden chamber selection that each had passed [17].

To verify the authenticity of the cell clones we are using, we performed wound healing assay to reconfirm the differing degree of migratory ability as documented. It is performed by making a restrained scratch on a nearly confluent culture of cells, to create uniform cell-free spaces that allows adjacent cells to migrate into the area. We measured the original width of the area immediately after the scratch as 100%, and for the subsequent time points, the width of the same locations were measured again to

obtain the remaining percentage of cell-free space. The wound closure percentage was measured by subtracting the latter remaining percentage of cell-free space from 100%, the original space immediately after scratching (Figure 2A).

According to our data, there are not so different wound closure percentage in CL1-0 and CL1-1 which presented lower rate of migration. In contrast, the wound closure percentage of CL1-5 is about 4-fold higher than the other two sublines (Figure 2B). Additionally, to ruled out the doubt that the differences between their wound closure percentage were the results of differences in their proliferation rate, we performed a cell proliferation analysis by counting viable cells using Trypan Blue exclusion assay at the end time point for the wound closure assessment (24h post seeding) from 3 independent experiments. In both experiments we verified that the ability of CL1-5 to migrate into spaced regions resulted in significantly faster wound closure, despite it did not display the faster proliferative index (Figure 2C).These results already confirmed the migratory abilities of CL1-0, CL1-1 and CL1-5as originally documented properties. CL1-5 as the representative of high metastatic potential, and CL1-0, CL1-1 as the representative of low metastatic potential, they are ideal tests models for MD-CaMP.

Fibronectin expression of CL1-0, CL1-1,CL1-5

Fibronectin plays a major role in oncogenic transformation, contributing to cancer cell growth and migration. Furthermore, higher level of fibronectin is correlated with cancer metastasis. In MD-CaMP, fibronectin is the indicator for analysis of cancer metastatic potential which depends on the characteristics of chitosan capable of modulating cell attachments through its interaction with fibronectin [15].

With three testing cell model representing differential degree of metastatic potential, we next wanted to check if the metastatic potentialof CL1-0, CL1-1 and CL1-5 were related to their fibronectin expression. Data from western blot probed with fibronectin antibody showed CL1-5 with higher metastatic potentialhad higher fibronectin expression level than CL1-0, CL1-1 cells (Figure 3).

Correlation of metastatic potential with rate of detachment on chitosan

By the adjustment of medium pH value, one can control cell attachment on chitosan depending on the interaction between extracellular fibronectin and chitosan. When the environmental pH increased which make chitosan become negatively charged, cell attachment on chitosan may decrease because the electro affinity between negatively charged fibronectin and chitosan becoming negatively charged decrease. Based on the concept, we tested if the highly migratory CL1-5 and lowly migratory

CL1-0, CL1-1 with differential level of fibronectin expression presented differential rate of detachment on chitosan coated MD-CaMP when raising environmental pH value.

CL1-0, CL1-1 and CL1-5 were seeded separately on MD-CaMP to test cell detachment when the culture conditions were altered from pH 7.2 to 7.8, under a simulated blood flow infusion of physiological medium (8 mm s^{-1} in artery = 64 mL h^{-1} flow rate in our chip) through a micro-flow syringe pump into the MD-CaMP. Cells were infused by medium at pH 7.2 for 6 min as control, followed by infusion of medium at pH 7.8 for 6 min. After incubated in the environment at pH 7.8 for 35 min, cells were infused again for 6 min (Figure 4A). The time lapse phase contrast microscope was used to image cells remaining in the MD-CaMP at each time point before and after flow infusion. We quantified the number of cells attached per unit area in percentiles to the original number present in the same area (Figure 4B). Notably, results showed that there are no differences in cell detachments at pH 7.2, after the pH changed to 7.8, CL1-0 and CL1-1 still remained attached while the CL1-5 cells displayed substantial detachment from the chitosan surface (Figure 4C).

Since the interaction between chitosan and fibronectin decreased, the more fibronectin-dependent cells such as CL1-5 tended to detach from the chitosan coated surface more rapidly than CL1-0 and CL1-1 when pH value of medium changed from pH7.2 to pH 7.8 (Figure 4D). From this experiment we concluded that the design of

MD-CaMP and our operating scheme can efficiently discriminate cells with different degrees of metastatic ability.

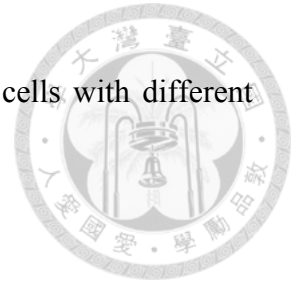

Selective fractionation of cells from a mixed population by their differential rate of detachment

Tumor is a heterogenous tissue containing many different types of cells and cells with different metastatic characteristics. Similarly, cells collected from biopsied specimens are mixed cell populations. If being able to measure the percentages of highly metastatic populations among whole cells, the metastatic potential of cancer can be predicted.

We have tested that MD-CaMP could discriminate cells with different degrees of metastatic ability. In the following experiment, we wanted to test the ability of MD-CaMP to fractionate cells according to their metastatic ability in CL1-1, CL1-5 co-cultured system. We labeled CL1-1 with MitoTracker Red, CL1-5 with CFDA and perform similar experiments as the last one. Labeled CL1-1 cells and CL1-5 cells were mixed and co-seeded on MD-CaMP and introduced buffered culture medium at pH 7.2 and 7.8 under infusion of physiological simulated blood flow through a micro-flow syringe pump. Cells were infused by medium at pH 7.2 for 10 min as control, followed

by 40 min of incubation before infusion of medium at pH 7.8 for 10 min (Figure 5A, B). Data indicated neither CL1-1 nor CL1-5 cells detached under simulated blood flow at pH 7.2, indicating a stable interaction between chitosan and the cellular fibronectin. However, after switching to pH 7.8, the percentile of attached CL1-5 cells decreased sharply, from 78% to almost none at the end of the simulated infusion. In contrast, CL1-1 maintained about 90% of the cells attached (Figure 5C). Taken together, our chip design is capable of discriminating between cells with differing metastatic potential, even in mixed cell populations as the clinical specimens are.

Altered cell morphology with pH

To exclude the possibly that the increase in medium pH may cause cellular damage that leads to detachment from the chitosan, we followed the change in cell morphology using DIC imaging. We found that the CL1-5 cells were still completely attached to the chitosan-coated surface after 60 min at pH 7.4. When the pH was switched to 7.8, the cells gathered and began to detach (Figure 6).

Differential attaching properties of CL1-0, CL1-1 and CL1-5 on chitosan surface

We have proven the abilities and advantages of MD-CaMP which is able to

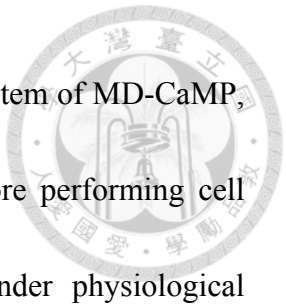

separate cells according to their metastatic ability. In the analysis system of MD-CaMP, cells have to be seeded previously on chitosan for overnight before performing cell detachment assay by infusion of culture medium at pH 7.8 under physiological simulated blood flow velocity. As a result, it takes more than one day for the whole assaying processes. We are thinking if time needed for MD-CaMP analysis can be shorten to improve the testing efficiency. Cell seeded on chitosan surface detach when raising environmental pH (higher than its pI) which makes chitosan become negatively charged because negatively charged extracellular fibronectin repels chitosan with the same electric property. We were wondering in normal cell culturing condition (pH 7.2-7.4) when chitosan is positively charged, if there would be differences in the rate of cell attachment due to differential degree of fibronectin adsorption on chitosan surface. We hypothesize that the negatively charged fibronectin which composes the extracellular matrices of cancer cells may be more prone to adsorb to positively charged chitosan.

Firstly we tested the attachment rate of CL1-0, CL1-1 and CL1-5 individually on chitosan coated cell culture dish. CL1-0, CL1-1 and CL1-5 were seeded equally on chitosan surface and washed at indicated time point (0, 1, 2, 3, 4, 5 hr after seeding)(Figure 7A). We quantified the number of cells remained after wash in percentiles to the original number of cells before wash. As seen in data, almost all

CL1-5 cells attached while about 60% of CL1-1 and less than 10% of CL1-0 attached after seeding for 4 hours, saying that cells with higher metastatic potential attached faster on chitosan surface (Figure 7B). From this experiment we discovered that cells with differential fibronectin expression could truly led to differential rate of cell attachment on chitosan surface as a result of differential degree of fibronectin adsorption on chitosan surface.

Cell fractionation of co-cultured CL1-0, CL1-1, CL1-5 by differential attachment properties on chitosan surface

Also in co-cultured system where equal amount of CL1-0, CL1-1 and CL1-5 were mixed and seeded on chitosan surface, CL1-5 attached much faster than CL1-1 which attached faster than CL1-0; however, when seeded on general TCPS (tissue culture polystyrene) dish as control, there were no differences in their attachment rate (Figure 8A, B). Data suggested chitosan was able to separate cells with different metastatic potential also by their differential rate of attachment. By means of assaying cell attachment instead of cell detachment on chitosan, we saved a lot of time spending on the whole analysis processes because there was no need for pre-seeding of cells and modulating pH of infused medium. These discoveries gave us a clue that we could

improve our analysis system based on cell attachment rate and reform MD-CaMP according to this concept to provide more efficient analysis for cancer metastatic potential.

Conclusion and Discussion

In this study, we proposed the design of a microfluidic device for detecting cancer metastatic potential with living specimens obtained from biopsy, and we have proved that MD-CaMP can fractionate cells with differential metastatic abilities from a mixed population of cancer cells simulating biopsy specimen. Our design constitutes the first example that integrates the control of both temperature and CO_2 for the maintenance and functional assay of live cancer cells in a microfluidic chip. We exploited that fibronectin expression of cancer cells can be an indicator for functional discrimination of cell metastatic ability by its physical interaction with pH-responsive chitosan which as a result alters cell adhesion properties on chitosan surface, to provide a rapid index for cancer metastatic potential. We expect that MD-CaMP can provide valuable information for the planning of optimal treatment clinically.

Microfluidics enables design flexibility, great reproducibility, fluidic control, reduced consumption of reagents and chemical waste, abbreviated duration of sample treatment, selective gas permeability and experimental feasibility. Being the principle part of this device, the microfluidic-based chip can render many benefits.

For examples, microfluidic chip is small enough to handle small specimens even few cells from fine needle biopsy, so the extra specimens is not required from patients for this test. Also, it is a portable device, hence the analytic processes can be easily

performed on bedside for on-site diagnoses. Additionally, because the manufacture of microfluidic chip is inexpensive, it can be massively produced and applied as a screening test for patients suspected with lung cancer and asked to get biopsy.

The outer CO_2 chamber surrounding cell culture chamber and the micro-temperature control system put under microfluidic chip serve as a miniaturized microfluidic cell incubator to maintain a basic growth environment that allows both cell culture in the atmosphere and recording cell images directly on this device. The micro-temperature control system offers a uniform and stable distribution of temperature (37 °C) in the area of cell culture. Meanwhile, $NaHCO_3$ solutions filled in the CO_2 chamber pass through the gas-permeable chamber wall made from PDMS providing a partial pressure of CO_2 that adjusts medium pH to a physiological condition. At the same time, the humidity of the external environment is maintained and the evaporation of the medium is slowed. This device combines the advantages of both commercial closed and perfusion-type microincubation image-chamber slides: little pollution and the possibility of modifying the medium or the addition of drugs, providing high-resolution cellular imaging more effectively than a plate or microwell imaging more effectively than a plate or microwell.

The pH-responsive chitosan coated on cell culture area discriminates cancer cells having differential metastatic potential through its electro affinity with extracellular

fibronectin that alters cell adhesion properties on chitosan surface. We are able to control cell attachment to and detachment from the surface of pH-sensitive chitosan via varying environmental pH either by bicarbonate buffered CO2 chamber maintaining physiological pH 7.2-7.4 or by the infusion of medium at pH 7.8. On one hand, with a varied rate of detachment of cells on chitosan surface, chitosan is an analytic platform for the discrimination of cancer metastatic potential. On the other hand, cells after analysis can be retrieved by the characteristic of pH responsive chitosan for downstream research, without any additional treatment. The detachment of cells from the surface of the substrate is at present mainly achieved with a conventional proteolytic enzyme treatment that might impair some cell functions and complicate the cell culture. In our case, cells were therefore grown and detached from the chitosan surface by controlling the pH of the environment; protease-based solutions, such as trypsin, are no longer required.

ECMs affect tumor cell behavior including metastasis. Abnormal ECM dynamic is well reported in clinical studies and it is a hallmark of cancer. Fibronectin is one of the extracellular matrix protein and its expression is positively correlated to metastatic potential of lung cancer. Fibronectin can thus be considered as an indicator for assaying lung cancer metastatic potential. In our cell models for testing, three human lung adenocarcinoma sublines CL1-0, CL1-1, CL1-5 with differential migratory abilities

have different degree of fibronectin expression. Besides, higher level of fibronectin also participates in metastasis of oral, breast cancers. Nevertheless, we chose the CL1 series for lung metastatic cancer model to test our device because of their well documented characteristics as a standardized lung cancer sublines representing progressive metastatic abilities. The use of MD-CaMP will not be confined to lung cancer.

Moreover, other ECM proteins have also been reported in the role of cancer progression. For instance, thickening and linearization of collagen fibers are often found in areas where active tissue invasion and tumor vasculature, suggesting that they play an active role in facilitating cancer invasion. Same as fibronectin, collagen or other ECM proteins are as well negatively charged in normal culture condition (pH=7), MD-CaMP can as a result be applied to sort different types of cancer cells with distinct composition and properties of ECMs also by the electro-interaction between negatively charged ECMs and pH-responsive chitosan. The future potential of MD-CaMP can include clinically usage as a quick screening tool widely for many kinds of cancer.

Reference

1. Mehlen, P. and A. Puisieux, *Metastasis: a question of life or death.* Nat Rev Cancer, 2006. 6(6): p. 449-58.
2. Stewart, B.W., et al., *World cancer report 2014*. xiv, 630 pages.
3. Jemal, A., et al., *Cancer statistics, 2004.* CA Cancer J Clin, 2004. 54(1): p. 8-29.
4. Mazzone, P., et al., *Bronchoscopy and needle biopsy techniques for diagnosis and staging of lung cancer.* Clin Chest Med, 2002. 23(1): p. 137-58, ix.
5. Velve-Casquillas, G., et al., *Microfluidic tools for cell biological research.* Nano Today, 2010. 5(1): p. 28-47.
6. Velve Casquillas, G., et al., *Fast microfluidic temperature control for high resolution live cell imaging.* Lab Chip, 2011. 11(3): p. 484-9.
7. Velve-Casquillas, G., et al., *A fast microfluidic temperature control device for studying microtubule dynamics in fission yeast.* Methods Cell Biol, 2010. 97: p. 185-201.
8. Forry, S.P. and L.E. Locascio, *On-chip CO2 control for microfluidic cell culture.* Lab Chip, 2011. 11(23): p. 4041-6.
9. Lu, P., V.M. Weaver, and Z. Werb, *The extracellular matrix: a dynamic niche in cancer progression.* J Cell Biol, 2012. 196(4): p. 395-406.
10. Cox, T.R. and J.T. Erler, *Remodeling and homeostasis of the extracellular matrix: implications for fibrotic diseases and cancer.* Dis Model Mech, 2011. 4(2): p. 165-78.
11. Jia, D., et al., *Development of a highly metastatic model that reveals a crucial role of fibronectin in lung cancer cell migration and invasion.* BMC Cancer, 2010. 10: p. 364.
12. Sun, X., et al., *The EDA-containing cellular fibronectin induces epithelial-mesenchymal transition in lung cancer cells through integrin alpha9beta1-mediated activation of PI3-K/AKT and Erk1/2.* Carcinogenesis, 2014. 35(1): p. 184-91.
13. Quail, D.F. and J.A. Joyce, *Microenvironmental regulation of tumor progression and metastasis.* Nat Med, 2013. 19(11): p. 1423-37.
14. Yeh, H.Y. and J.C. Lin, *Surface characterization and in vitro platelet compatibility study of surface sulfonated chitosan membrane with amino group protection-deprotection strategy.* J Biomater Sci Polym Ed, 2008. 19(3): p. 291-310.
15. Chen, Y.H., et al., *Control of cell attachment on pH-responsive chitosan surface by precise adjustment of medium pH.* Biomaterials, 2012. 33(5): p. 1336-42.
16. Chen, Y.H., et al., *Cell fractionation on pH-responsive chitosan surface.* Biomaterials, 2013. 34(4): p. 854-63.
17. Chu, Y.W., et al., *Selection of invasive and metastatic subpopulations from a human lung adenocarcinoma cell line.* Am J Respir Cell Mol Biol, 1997. 17(3): p. 353-60.

Figures

(A)

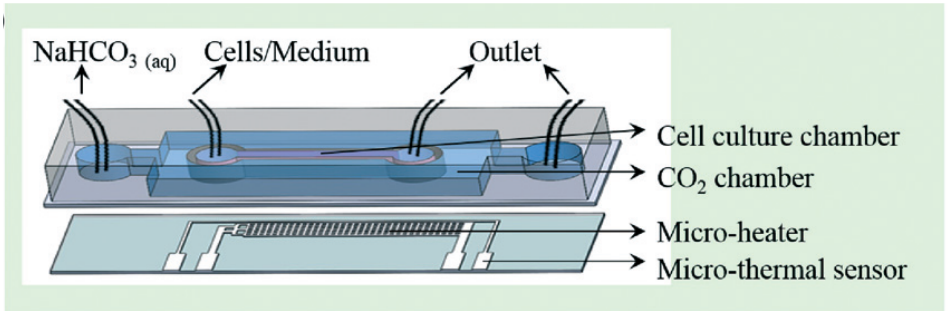

(C)

(B)

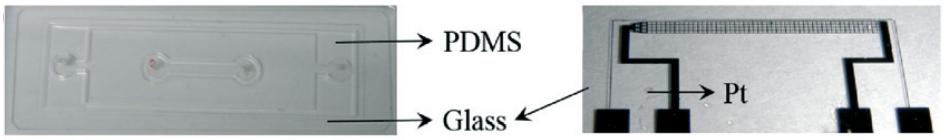

(E)

(D)

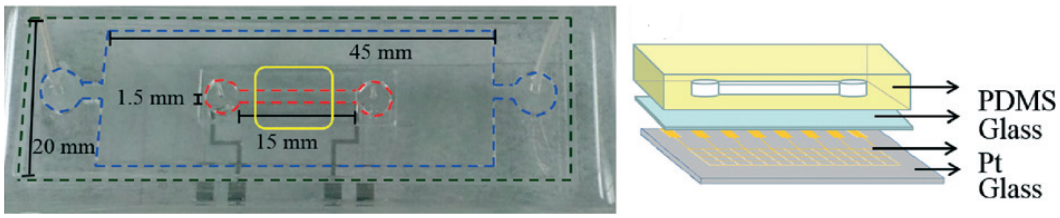

Figure 1. Design and fabrication of the microfluidic chip

(A) Schematic illustration of this device, MD-CaMP. MD-CaMP contains two parts: the micro-temperature control system and the main body of this device, microfluidic chip. Micro-temperature control system includes a micro-heater and a micro thermal sensor. The main body of this device, microfluidic chip, is composed of outer CO_2chambers and inner cell culture chambers.(B) CO2 and cell-culture chambers. (C) Pt micro-heater. (D) Top view of an assembled device. The red dashed line indicates the cell-culture area and between the blue and red lines is the CO2 chamber. The area marked by the yellow square box is the region for observing the cell behavior. (E) Side view of the material of each part. The transparent PDMS facilitates cell observation.

(A)

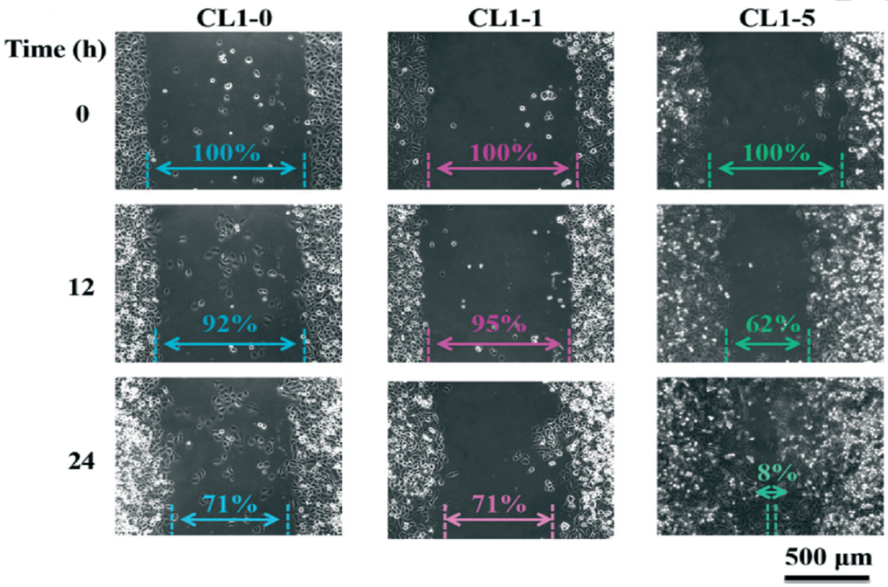

(B)

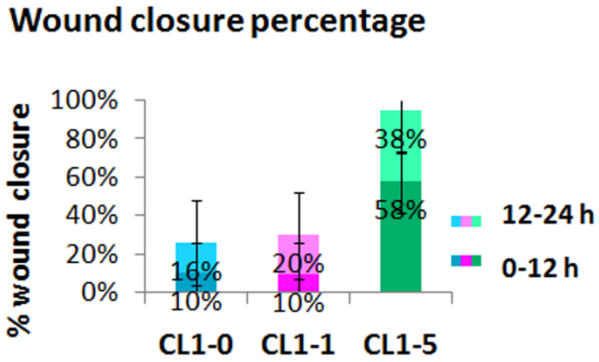

(C)

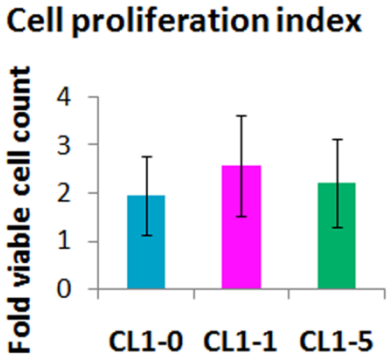

Figure 2. Migratory abilities of CL1 lung cancer sublines, CL1-0, CL1-1 and CL1-5

(A) Time-lapse images of live CL1 sublines CL1-0, CL1-1 and CL1-5 obtained with a phase-contrast microscope after the indicated intervals after standard wound-scratch procedures. The original width of the area immediately after the scratch was measured as 100%, and for the subsequent 12 and 24 hour, the width of the same locations were measured again to obtain the remaining percentage of cell-free space. (B) Mean wound closure fractions(as percentiles) from three independent experiments. (C) Fold viable cell count of CL1-0, CL1-1 and CL1-5 after 24 hours of culturing. Cell proliferation analysis was performed by counting viable cells using Trypan Blue exclusion assay at the end time point for the wound closure assessment (24h post seeding).

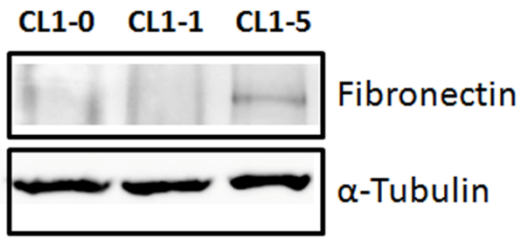

Figure 3. Level of fibronectin expression on CL1-0, CL1-1 and CL1-5

Western blot analysis of CL1-0, CL1-1 and CL1-5 with fibronectin and α-tubulin (as loading control) antibodies.

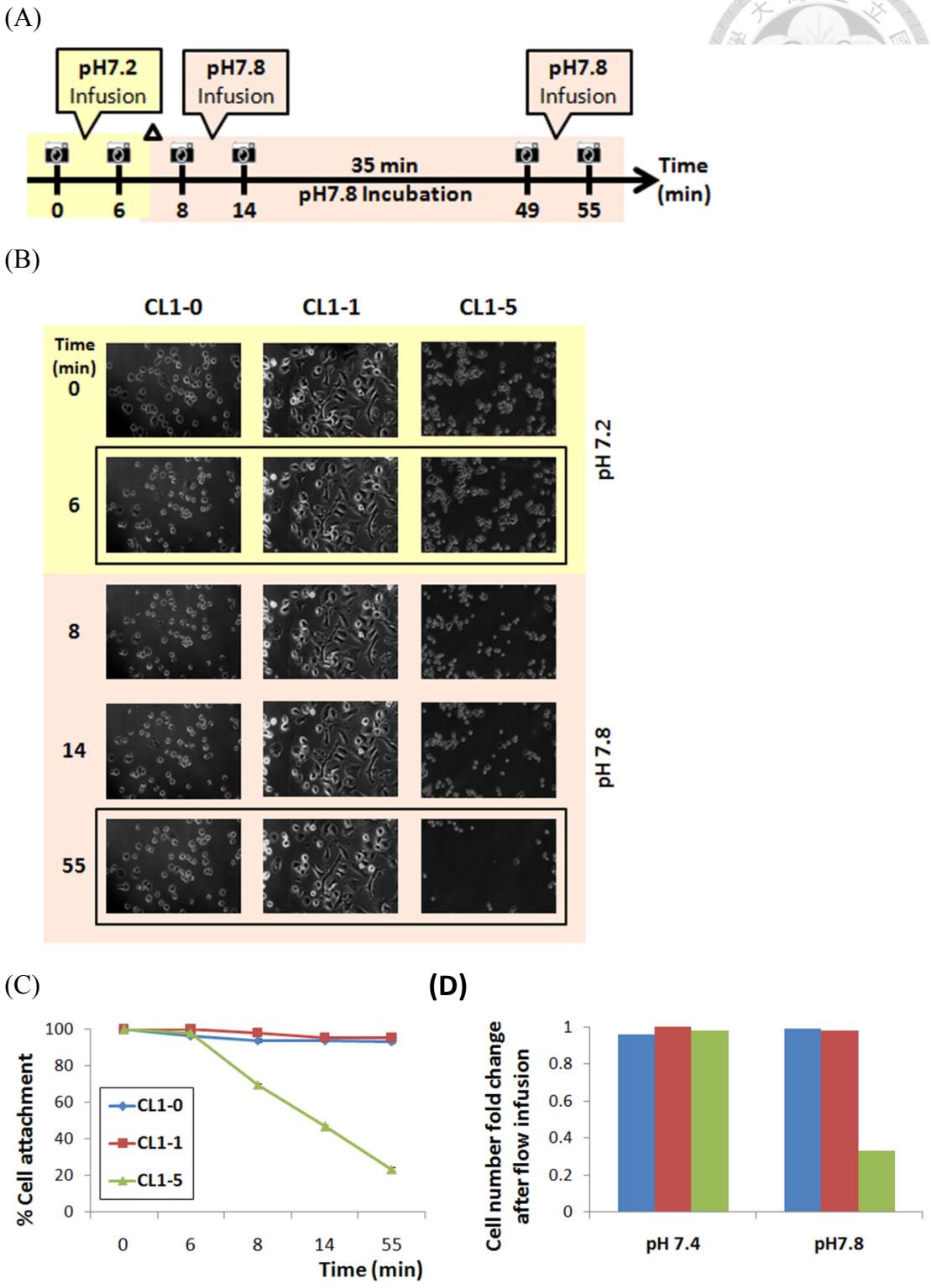

Figure 4.Cell detachment of CL1-0, CL1-1, CL1-5assessed by MD-CaMP

(A) Experimental scheme of cell detachment on MD-CaMP. Cells seeded in MD-CaMP were infused by medium at pH 7.2 for 6 min as control, followed by infusion of medium at pH 7.8 for 6 min. After incubated in the environment at pH 7.8 for 35 min, cells were infused again for 6 min. The velocity of flow we infused

simulated physiological blood flow (8 mm s−1 in artery = 64 ml h^{-1} flow rate in our chip). (B) Time-lapse images of the cells in the MD-CaMP upon infusion of buffered media. (C) Quantitative representation of the percentage of cells that remained attached on the chitosan surface at the indicated times. (D) The fold change of cell fractions attached while infusing with pH 7.4 medium as compared to pH7.8 medium.

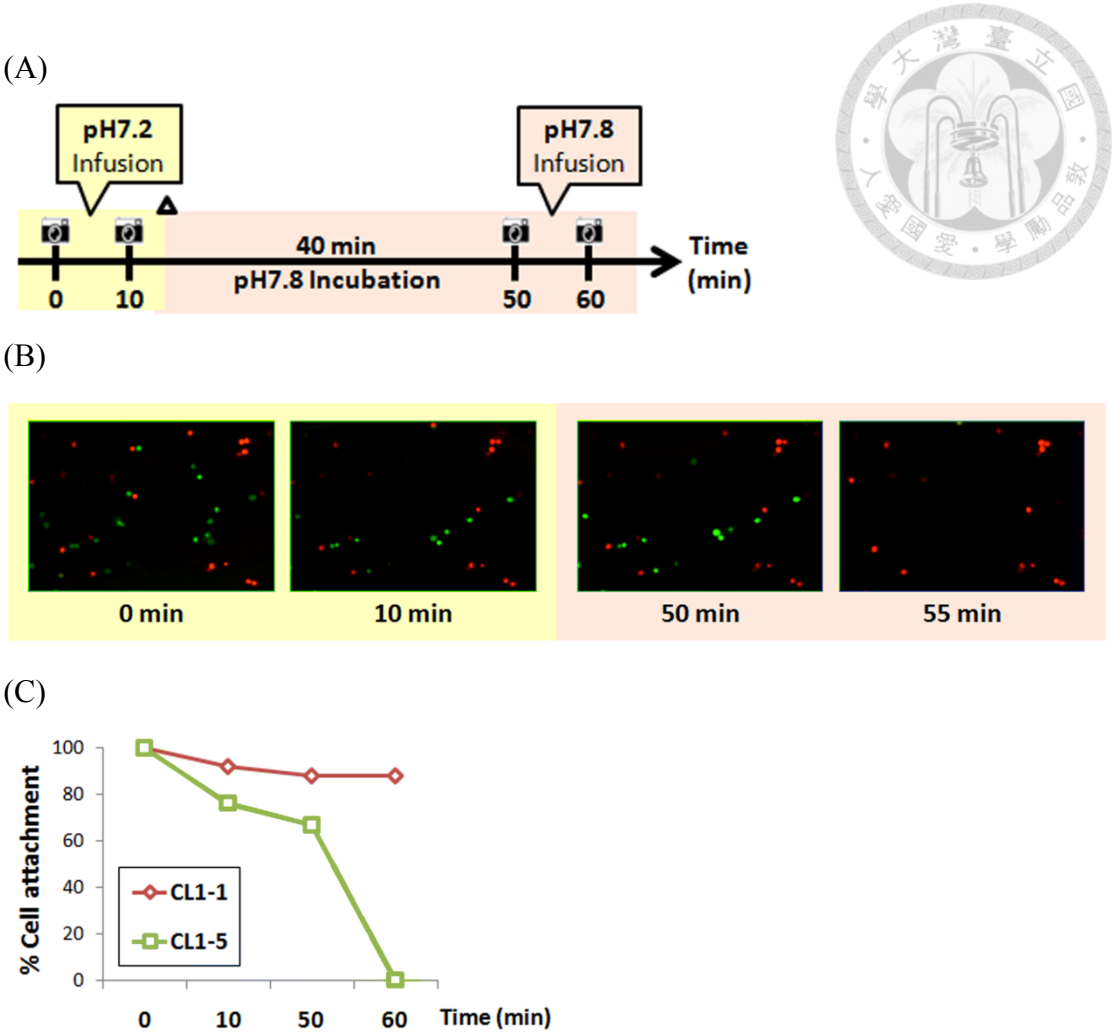

Figure 5. Live cell fractionation in CL1-1,CL1-5 co-cultured system

(A) Experimental scheme of cell detachment in CL1-1 and CL1-5 co-cultured system on MD-CaMP. Cells seeded in MD-CaMP were infused by medium at pH 7.2 for 10 min as control, followed by 40 min of incubation before infusion of medium at pH7.8 for 10 min. (B) Time-lapse images of fluorescently labeled CL1-1 cells (red) and CL1-5 (green) cells co-cultured in the MD-CaMP. Buffered media at the indicated pH were infused in indicated time interval. (C) Quantification of the cells that remained attached to the same region of the chitosan surface was recorded using fluorescence microscopy at the indicated time points.

(A)

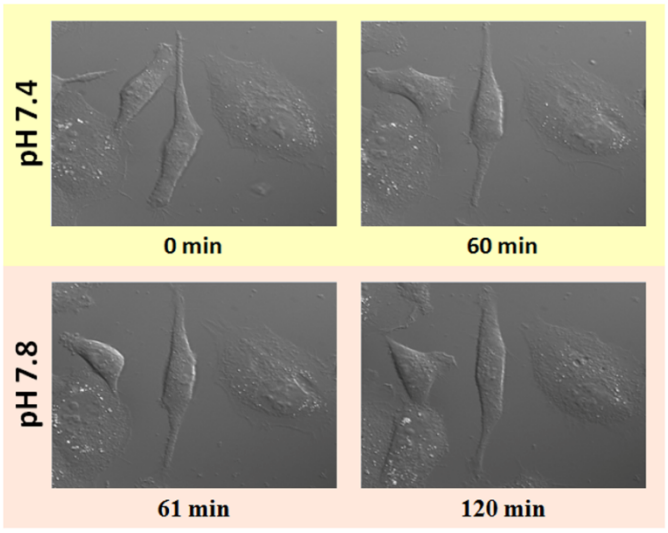

Fig. 6 Morphological change of CL1-5 cells on chitosan surface after incubation in different pH media as monitored by DIC microscopy

CL1-5 cells seeded on chitosan surface were incubated in medium at pH 7.4 for 60 min followed by incubation of medium at pH 7.8 for another 60 min.

(A)

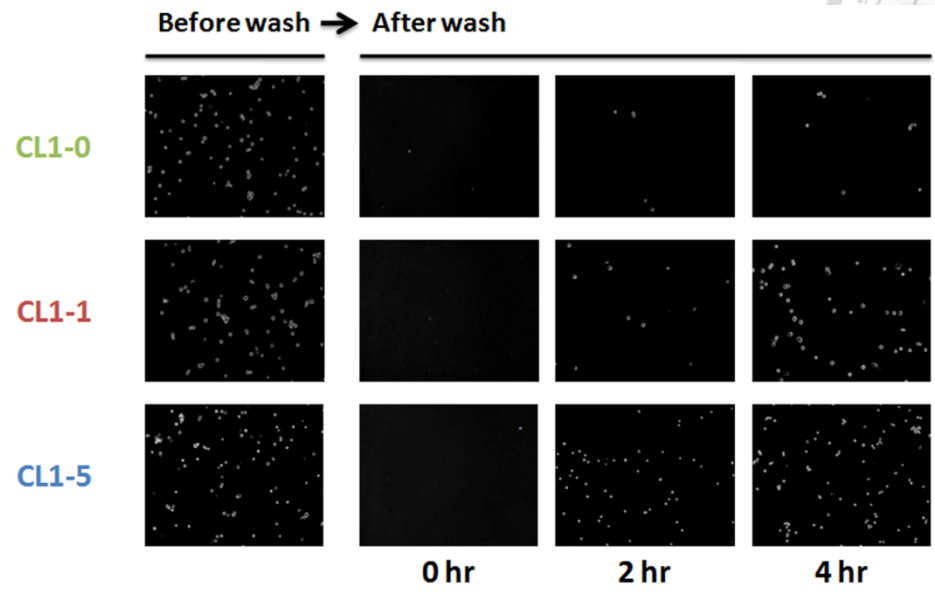

(B)

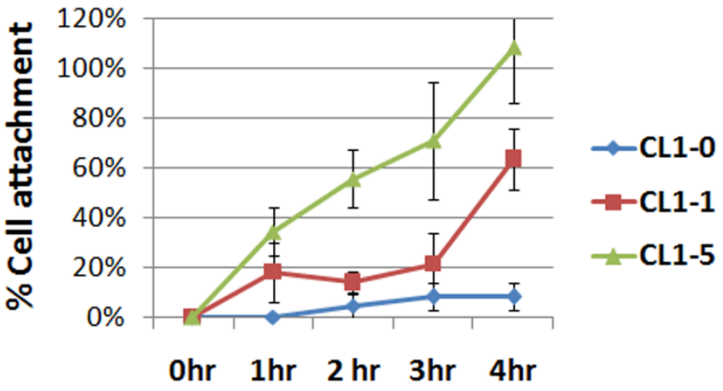

Fig. 7 Cell attachment of CL1-0, CL1-1, CL1-5 on chitosan surface

(A) Images of CL1-0, CL1-1, CL1-5 seeded separately on chitosan surface before wash and wash after 0, 2 and 4 hr of culturing. (B) Quantification of the cells that remained attached on chitosan surface after wash at indicated time point.

(A)

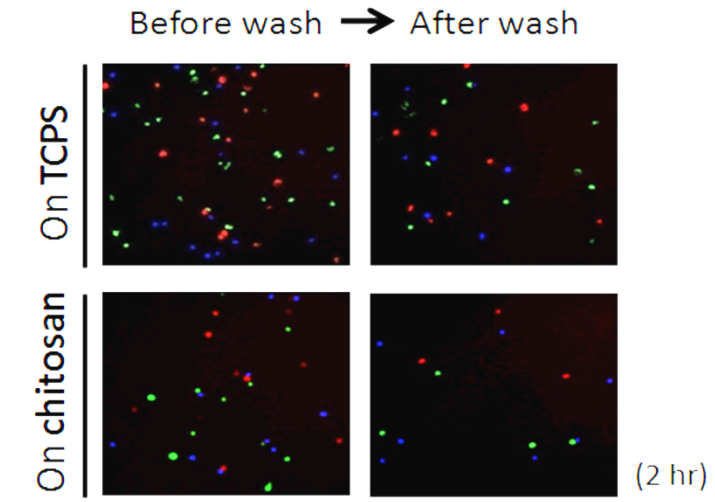

(B)

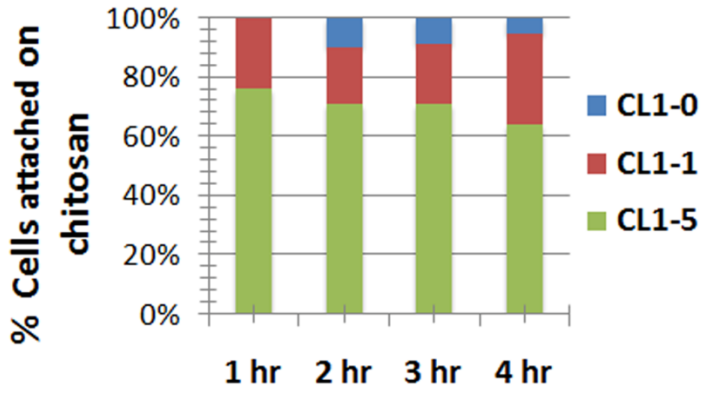

Fig. 8 Cell fractionation of co-cultured CL1-0, CL1-1, CL1-5 by differential attachment properties on chitosan surface

(A) Images of fluorescently labeled CL1-0 (blue), CL1-1 (red) and CL1-5 (green) cells co-seeded on general TCPS dish (as control) or chitosan surface before and after wash. (B) Quantification of percentages of each sublines attached on chitosan surface after wash at indicated time point.

Appendix

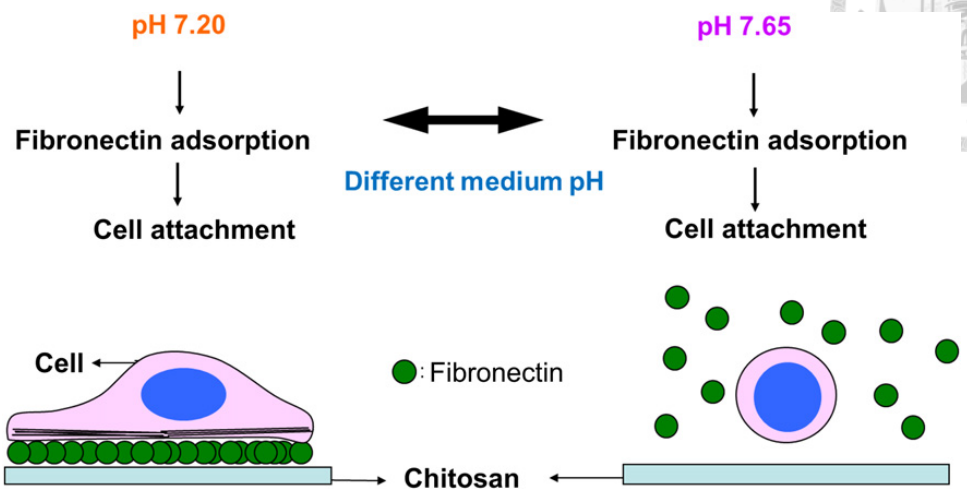

Appendix 1. Schematic representation of the relationship among medium pH, fibronectin adsorption, and cell attachment on chitosan.

研究二 SIK2 藉由磷酸化 CAPS2 調控胰島素分泌之探討

摘要

動物體的各種器官之協同運作，需仰賴內分泌系統對細胞之調節作用。胰島素即係一種負責控制血糖濃度之內泌素。當胰島素的生成或分泌發生異常，抑或是體內細胞出現胰島素失敏之現象，便可能引起糖尿病。佔總糖尿病患數 90 – 95% 之第二型糖尿病，其起因爲體細胞逐漸產生胰島素抗性，進而造成胰島素過量分泌之代償作用，終而導致 β 細胞劇烈死亡。因此，改善其病徵之方法可為刺激胰島素分泌及抑制 β 細胞凋亡。Salt inducible kinase 2 (SIK2) 係一屬 AMPK 族群之酵素，於 β 細胞中調控胰島素之分泌，並藉由抑制 CREB-mediated IRS-2 基因表現，促使 β 細胞凋亡。本研究室先前研究指出，SIK2 可透過其磷酸酶活性控制 β 細胞中胰島素小泡之遷移及分泌，而抑制 SIK2 磷酸酶活性可增加胰島素之分泌。為進一步探討 SIK2 對胰島素分泌調控之機轉，吾人以 Scansite 網站資料庫預測，發現 calcium-dependent activator protein for secretion 2 (CAPS2) 蛋白具有 SIK2 之磷酸化目標序列，可能為 SIK2 之下游調控因子。欲了解 SIK2 是否會透過 CAPS2 影響胰島素分泌，本研究首先確認 SIK2 及 CAPS2 均於 β 細胞中表現，再以免疫沈澱法驗證其交互作用，並以 *in vitro* kinase assay 證明 CAPS2 確為 SIK2 之磷酸化目標。然而，吾人實驗結果亦顯示於 SIK2 及 CAPS2 共同過量之小鼠 β 細胞中，SIK2 可透過 CAPS2 強化細胞對葡萄糖刺激之反應。綜合上述，本研究結果指出 SIK2 可藉磷酸化 CAPS2 調控 β 細胞中胰島素之分泌，然其中詳細之分子機制，尚待未來進一步研究發掘。

Study II: Identification of CAPS2 as a downstream target of SIK2 in regulating insulin secretion

Abstract

Through the endocrine system, communications between cells in various tissues in our body are well coordinated to drive a variety of physiological events properly. Insulin, one of endocrines, is secreted in response to elevated blood concentration of glucose, thereby keeps blood sugar level within certain range. Either failures of production and secretion of insulin, or cellular insulin insensitivity could result in diabetes mellitus. Type 2 diabetes (T2D) accounting for 90–95% of those with diabetes, is caused by the cellular resistance to insulin stimulation which leads to progressive insulin secretion defect in order to compensate for the less responsive reactions, and finally massive death of β cells. Ways to treat T2D are to stimulate more insulin secretion and to inhibit β cell death. Salt inducible kinase 2 (SIK2), a member of AMPK family, plays important roles in both β cell survival as well as insulin secretion. SIK2 has been reported to suppress β cell survival by repressing CREB-mediated IRS-2 gene expression. Our group found that SIK2 is expressed in insulin-producing β cells and regulates dynamics of insulin secretion via its kinase activity. Inhibition of SIK2 kinase activity resulted in vesicle mobilization to the membrane and increased insulin release. To further understand the machinery of the regulation of insulin secretion by SIK2, we

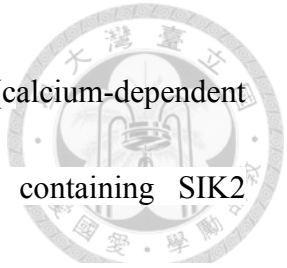

applied Scansite database search program and found that CAPS2 (calcium-dependent activator protein for secretion 2), the vesicle related protein containing SIK2 phosphorylation consensus motif, was considered as a putative downstream substrate of SIK2. Herein, we firstly confirmed the physiological protein interaction between CAPS2 and SIK2, and found the interaction was correlated to SIK2 kinase activity. In addition, our *in vitro* kinase assay results provide clear evidences to show that CAPS2 is the direct substrate of SIK2. However, in SIK2/CAPS2 overexpressing mouse primary β cells, SIK2 might regulate insulin secretion via CAPS2 by sensitizing the responses to glucose in β cells. Taken together, our findings suggest that the function of CAPS2 is involved in insulin secretion and is regulated by protein kinase SIK2. Future studies are needed to reveal the mechanisms of the SIK2/CASP2 pathway in controlling insulin secretion.

Introduction

Definition, classification, cause and prevalence of diabetes mellitus

Diabetes mellitus is a group of metabolic diseases characterized by hyperglycemia resulting from defects in insulin secretion, insulin action, or both [18]. The patients' bodies fail to release enough amounts of the blood glucose-lowering hormone insulin, or/and the target organs is unable to respond to insulin while blood-glucose level increased. The chronic hyperglycemia of diabetes may leads to long-term damage especially to eyes, kidneys, nerves, heart, and blood vessels, causing retinopathy, renal failure, cardiovascular symptoms and so on.

The major cases of diabetes are classified into two categories. Type 1 diabetes, insulin-dependent diabetes (IDDM), also termed Immune-mediated diabetes or juvenile-onset diabetes, accounts for 5–10% of those with diabetes [19]. It is arose from the autoimmune destruction of the pancreatic β cell, leading to absolute insulin deficiency. Patients suffering from type 1 diabetes rely on multiple daily insulin injection or insulin pump therapy with daily blood sugar monitoring or islet transplantation to survive [20]. Type 2 diabetes, noninsulin-dependent diabetes (NIDDM), also referred to as adult-onset diabetes, accounts for 90–95% of those with diabetes. It is caused by the resistant target cells to insulin action, leading to progressive

insulin secretion defect in order to compensate for the resistance, and finally β cell apoptosis [21]. Insulin normally turns down gluconeogenesis to keep blood sugar levels from rising, but in people with insulin resistance, blood sugar levels are elevated because gluconeogenesis continues when it shouldn't [http://www.science20.com]. Patients with type 2 diabetes depend on medications that stimulate more insulin secretion or inhibit glucose production and release, along with special attentions on diet and physical activities. Drugs such as metformin, the first-line drug for treatment of type 2 diabetes, lower blood glucose by suppressing living releasing glucose and by increasing insulin sensitivity. Other drugs like Sulfonylurea works on increasing insulin production and secretion [22, 23].

The prevalence of diabetes worldwide was reported to be 2.8% in 2000 and will rise to 4.4% in 2030. The total number of people with diabetes was reported to rise from 171 million in 2000 to 366 million in 2030.Similar trend has also happened in Taiwan that there was a more than 70% increase in the total diabetic population, or a 35% increase in the standardized prevalence rate from 2000 to 2009 [24, 25]. Diabetes has becoming an ever greater public health problem, so it is important to develop therapies to prevent the development of or treat existing diabetes.

Secretory pathway, distinct pools and biphasic secretion of insulin vesicles in pancreatic β cells

Insulin, the only blood glucose-lowering hormone in the body, plays key roles in glucose homeostasis and maintenances of blood sugar level. It is produced and secreted by pancreatic β cells in islets of Langerhans. Roughly speaking, insulin secretion is a process that involves the packaging of insulin granules, the trafficking of granules to the plasma membrane, and the exocytotic fusion of granules with plasma membrane. After synthesized in the ER and underwent maturation steps, it is packaged in the Golgi into secretory granules allowing further processing to biologically active insulin [26]. Peptide secreting endocrine cells such as chromaffin cells and beta cells pack and store hormones in large dense core vesicles (LDCVs), which contain a big core that is electron-dense under the electron microscope [27].

Insulin secretion is controlled by β-cell electrical activity [28].When the blood glucose level is raised after eating, β cells sense higher ATP production metabolized by glucose. Increased cytosolic ATP/ADP-ratio result in closure of ATP-sensitive potassium-channels (K_{ATP}-channels) in the plasma membrane, which leads to depolarization of the cell and activation of the voltage dependent calcium-channels (VDCC). The elevated cytosolic calcium concentration due to influx of calciumion through VDCC then triggers exocytosis and insulin secretion [29].

The secretory vesicles in beta cells can be functionally divided into two distinct pools, readily releasable pool (RRP) and reserve pool (RP), by their release competence

and proximity to the plasma membrane [30]. Each beta cell comprises more than 10,000 insulin-containing LDCVs, but only a small fraction (~ 1%) of these belongs to RRP, which can be released immediately without any further modification upon calcium influx. While the remainder (~99%) which belongs to RP requires a series of ATP-, calcium-, and temperature-dependent mobilization to the plasma membrane to refill the emptied RRP. Recruitment of granules from RP to RRP is a relatively slow process (~ 5 granules/sec., compared with the exocytotic burst of 700 granules/sec.) [31, 32]. The depletion of RRP takes less than a second, whereas its refilling takes up to a minute [33]. Glucose-stimulated insulin exhibits a characteristic biphasic pattern, consisting of a rapid and transient first phase followed by a slowly developing and sustained second phase [34]. The first phase burst secretion occurs within 10 minutes and a second phase can last 2-3 hours. The biphasic insulin secretion reflects the distinct pools of vesicles. The early rapid component (first phase) involves exocytosis of RRP, while the sustained component (second phase) corresponds to the balance of released RRP by mobilization of new granules from the reserve pool [35] .

Type 2 diabetes features defected insulin action and inability of β-cells to secrete enough insulin to maintain glucose homeostasis. It is characterized by the selective loss of first phase and a reduction of second phase in insulin secretion. Researchers was considering whether the secretory defect seen in type II diabetes results either from

incomplete closure of the K_{ATP} channels or interference with the mobilization of granules into the RRP [34]. In addition, restoration of first phase insulin secretion has been shown to improve blood glucose in type II diabetes by suppressing hepatic glucose production and having insulin sensitive tissue readily take up glucose [36]. Clinical treatments of type 2 diabetes focus on inhibiting glucose release from liver, increasing insulin sensitivity as well as stimulating more insulin release, so an understanding of insulin vesicle trafficking and secretion may lead to novel therapeutic strategies [37].

Roles of SIK2 in metabolism and insulin function

Salt Inducible Kinase 2 (SIK2) is among plenty of proteins appealing to us as the key molecule for studying the underlying mechanism in insulin secretion due to its multiple roles in metabolism and insulin function.

SIK2, with SIK1 and SIK3 are three isoforms of SIK that was first cloned from the adrenal glands of rats fed a high salt diet. SIKs are serine/threonine protein kinases which belongs to AMPK (AMP-activated protein kinase) family, essential regulators of cellular metabolism and energy homeostasis [38].

SIK2 is highly expressed in adipose tissue, while SIK1 is abundant in adrenal glands [5–7] and SIK3 has ubiquitous expression pattern [39, 40]. SIK2 has been

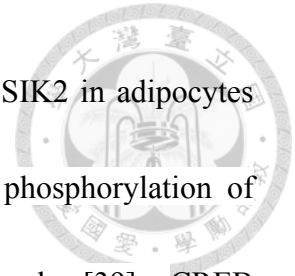

reported to play many roles in metabolic functions. Expression of SIK2 in adipocytes might modulate the efficiency of insulin signal transduction via phosphorylation of IRS-1 at Ser794, causing insulin resistance in diabetic animals [39]. CREB (cAMP-response element-binding protein) is required for beta cell survival by driving its direct target, IRS2 gene [41]. CREB also turns on genes for gluconeogenesis in liver during fasting to maintain blood sugar levels. However, SIK2 suppresses beta cell survival and gluconeogenesis by repressing CREB-mediated gene expression via phosphorylation of CREB-coactivator, TORC2, at Ser171, which results in binding of 14-3-3 proteins on TORC2 and thus confines its translocation to nucleus. Yet phosphorylation activity of SIK2 was decreased in response to cAMP by PKA through phosphorylation at SIK2 Ser587 that is important for TORC2 nuclear entry [42]. Overexpression of SIK2-S587A non-phosphorylatable mutant inhibited the *PGC-1α* and *UCP-1* gene expression, indicating the importance of SIK2-TORC2 cascade in regulation of insulin signaling in brown adipose tissue [43]. Furthermore, SIK2 is critical in the regulation of lipid homeostasis and adipogenesis in vivo, and phosphorylation at SIK2-Ser358 is involved in lipid metabolism [44].

Besides metabolic roles, SIK2 has been reported in diverse biological scenarios, including the regulation of neuronal survival after OGD (oxygen and glucose deprivation) via TORC1-CREB, the repression of melanogenesis, requirement for

mitotic spindle formation and so on [45-47].

The expression and function of SIK2 in pancreatic β cell in regulating insulin secretion

In pancreatic β cell, AMPK family is a fundamental regulator of insulin secretion [48]. Nevertheless, the function of AMPK-related kinase, SIK2, in pancreatic β cell to regulate insulin secretion has yet been published until March, 2014 [49]. Sakamaki's group points out SIK2 but not SIK1 or SIK3, is specifically required in β cell for insulin secretion. The SIK2–p35–PJA2 complex plays essential roles by which SIK2 phosphorylates p35 and begins its ubiquitination through PJA2 thus promote insulin secretion. In their *Sik2* adult β cell knockout mice model, ablation of *Sik2* resulted in accumulation of p35 causing glucose intolerance and impairment of insulin secretion by blocking calcium ion influx [49]. However, the functional modification on SIK2 kinase activity in controlling its behavior was not mentioned.

Our group also recognized the important position of SIK2 in insulin secretion and put a lot of efforts on studying its mechanism though our results were not exactly the same as Sakamaki's. In our study, we also discovered that SIK2 rather than SIK1 and SIK3 was expressed in pancreatic islets mainly in insulin producing cells (Appendix 1).

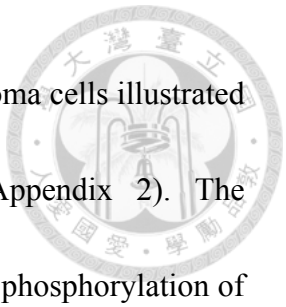

Subcellular fractionation experiment of insulin vesicles from insulinoma cells illustrated that SIK2 was associated with insulin containing LDCVs (Appendix 2). The well-characterized mode of regulation for SIK2 kinase activity is the phosphorylation of its activation T-loop Thr175 by LKB1, which is required for SIK2catalytic activity, as demonstrated by lack of activity in the Thr175Ala mutant[50]. In contrast, its kinase activity is inhibited by PKA-dependent phosphorylation of SIK2 at Ser587, which suspends the repression on CREB activity due to inability to phosphorylate TORC [39]. Previously our group found that SIK2-S587 was expressed in pancreatic islets and co-localized with insulin vesicles. In addition, we have provided the evidences that SIK2 was phosphorylated by cAMP dependent PKA phosphorylation on Ser587 upon glucose stimulation (Appendix 3). The kinase active SIK2-T175 and kinase inactive SIK2-S587 had distinct subcellular distribution that SIK2-T175 appeared in insulin vesicle around nuclear peripheral, while SIK2-S587 appeared in insulin vesicle near plasma membrane seemed to be readily releasable after glucose stimulation. Besides, treatment with 0.3 μM compound C, a selective SIK2 kinase inhibitor, not only increased insulin secretion but triggered movements of insulin vesicles toward plasma membrane (Appendix 4). In our view of point, we suggested that SIK2 participates in the regulation of insulin secretion via its kinase activity. In other words, we hypothesized that SIK2 regulates insulin secretion via phosphorylating “someone” on

the vesicle.

CAPS2 as a putative substrate of SIK2 in regulation of insulin secretion

The Scansite database search program at web site http://scansite.mit.edu helped us investigate the putative substrates of SIK2 by the referenced SIK2 phosphorylation motif：(Hy){(B)X or X(B)}XX(S/T)XXX(Hy), where S/T is the phosphorylatable Ser or Thr, and (Hy) and (B) are hydrophobic and basic residues, respectively. Vesicle related proteins that contain more than two of the putative SIK2 phosphorylation sites were set as searching criteria. Among many of the matched proteins, we chose those with reported roles in insulin secretion and noticed calcium-dependent activator protein for secretion 2 (CAPS2), having many putative target sites may be a potential downstream substrate of SIK2 (Appendix 5).

CAPS family (Calcium dependent activator protein for secretion) which comprises two members, CAPS1 and CAPS2, are cytosolic proteins that also peripherally associated with the plasma membrane, as well as the membrane of large dense core vesicles (LDCVs) [51, 52]. Involved in calcium-dependent exocytosis of LDCVs, CAPS proteins modulate the secretion of neurotransmitters, neuropeptides, hormones by mediating priming and the calcium-triggered fusion of secretory vesicles with the

plasma membrane in endocrine and neuroendocrine cells. As with Munc13s, CAPSproteins are identified as vesicle priming factors that interact with SANRE proteins and thereby promote SNARE-mediated membrane fusion [53, 54].

Both CAPS1 and CAPS2 share a similar domain structure, including a dynactin interacting domain (DID), a C2 domain, a pleckstrin homology (PH) domain, a MUN domain, and a C-terminal membrane-association domain [52]. C2 domain is a known protein motif involved in calcium and phospholipid interactions. PH domain is essential for regulation of exocytosis, as well as phospholipid binding in the plasma membrane. MUN domain represents the binding for the t-SNARE syntaxin and facilitates SNARE complex assembly [55].They have a strong expression in the (neuroe)endocrine tissues and also co-express in several tissues, however their functional differences remain to be clarified [56].

CAPS2 is a highly homologous paralog of CAPS1 as sharing > 80% amino acid identity. Molecular functions of CAPS2 in the roles of regulation LDCV exocytosis from PC12 cells are largely redundant with CAPS1 [57]. It was also reported that CAPS2 participated in the secretion of brain-derived neurotrophicfactor (BDNF) and neurotrophin-3 (NT-3) from cerebellar granule cells [58]. In addition, *Caps2*knockout mice not only have impaired BDNF release but also show autistic-like cellular and behavioral phenotypes [59].

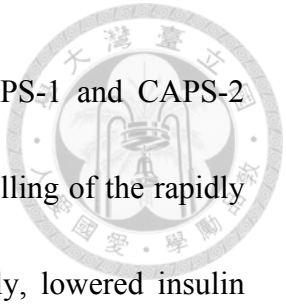

In the regulation of endocrine function, deletion of both CAPS-1 and CAPS-2 leads to a severe deficit in LDCV secretion because of a deficit in filling of the rapidly releasable pool (RRP) in mouse chromaffin cells [60]. Additionally, lowered insulin secretion from isolated pancreatic islets and reduced exocytosis from β cells was observed in $CAPS2^{-/-}$ and $CAPS1^{+/-}$,$CAPS2^{-/-}$ mice. CAPSs ablation not only led to systemic glucose intolerance *in vivo*, but resulted in suppression of glucose stimulated insulin secretion and over-secretion of glucagon *in vitro*. These phenomena of CAPSs ablation mimic the hormonal defects in type 2 diabetes. The study on the regulation between CAPSs and insulin secretion suggested that CAPS proteins serve as important modulators of LDCV-mediated insulin secretion in β cell exocytosis and granule stability.

Aim

SIK2 regulates insulin secretion through its kinase activity in pancreatic β cells. In this study, we aim to determine whether CAPS2 is the downstream substrate of SIK2 and how their interactions participate in insulin secretion.

Materials and Methods

Isolation of pancreatic islets

Pancreatic islets were isolated from 20-week-old male ICR mice followed the method described previously with modifications [61]. Mice were sacrificed by dislocation and its abdomens were opened with standard scissors. By using a Johns Hopkins Bulldog clamp, the end of the common bile duct before its entrance to small intestine was clamped off. The clamped common bile duct was cannulated by a 30 gauge 0.5 in. needle and injected with 1 mg/ml of collagenase Type V (032-17854, Wako Pure Chemical Industries). After injection, the inflated pancreas was collected and incubated with 2 ml collagenase solution in 37°C shaking water bath for 10 minutes followed by centrifugation (300xg, 4°Cfor 5 minutes). Pancreas pellets were washed with HBSS and undigested tissues were removed with the sieve. Remaining tissues in sizes larger than 70 μm were collected with a cell strainer and stored in RPMI medium (11875, Gibco, USA) supplemented with 10% FBS and 1% P/S. Islets were then collected under microscope for primary culture or fixed with 4% paraformaldehyde (43368, Alfa Aesar) in PBS for wholemount staining.

Cell culture

For primary culture of islet cell, cells were maintained in RPMI 1640 medium (Invitrogen) supplemented with 10% fetal bovine serum 1% P/S at 37°C in a 5% CO_2 humidified atmosphere. Cultured medium should be replaced within 2 weeks.

For HEK 293T cell, cells were maintained in DMEM medium (Invitrogen) supplemented with 10% fetal bovine serum and 1 mM sodium pyruvate at 37°C in a 5% CO_2 humidified atmosphere.

Antibodies

Mouse monoclonal Insulin antibody (cell signaling, #8138), Rabbit polyclonal Insulin antibody (cell signaling, #4590), Goat polyclonal CAPS2 antibody (Senta Cruz, sc-65014), SIK2-S901 (provided by Dr. Sheng-Chung Lee, Institute of Molecular Medicine and Clinical Medicine, College of Medicine, National Taiwan University), Mouse monoclonal C-Myc antibody (Senta Cruz, sc-40), Rabbit polyclonal Phospho-Threonine antibody (cell signaling, #9381)

Immunofluorescent staining:

For islet cells grown on glass cover slides, cover slides were picked up carefully from cultured medium and washed with 1× D-PBS followed by fixation with 4%

paraformaldehyde for 10 min. The cells were perforated with perforation buffer (0.3% Triton-X-100 in 1× D-PBS) for 10 min and blocked with blocking buffer (0.2% BSA and 0.1% Triton-X-100 in 1× D-PBS) for over 30 min, then probed with indicated primary antibodies (Insulin (Ms) 1:800, Insulin (Rb) 1:100, CAPS2 1:50, SIK2-S901 1:50, C-Myc 1:50) on 4°Covernight. After that, cover slides were washed with wash buffer (0.1% Triton-X-100 in1× D-PBS)and 1× D-PBS once. Secondary antibodies (Alexa 488-conjugated goat anti-rabbit IgG, Alexa 594-conjugated goat anti-mouse IgG, Alexa 488-conjugated donkey anti-goat IgG, Alexa 594-conjugated donkey anti-rabbit IgG (Invitrogen)) with 1:500 dilution were probed against primary antibodies for 2 hour and cell nucleiwere counterstained with Hoechst 34580 (Invrogen, H21486) for 10 minutes. Cover slides were washed again with1× D-PBS once and mounted with mounting buffer (90% glycerol in 1× D-PBS) for observation.

For mouse pancreas FFPE section, sections were de-paraffinized in xylene for 30mins followed by redydrated in graded ethanol from 100%, 100%, 95%, 70% for each 5 minutes and eventually in desterilized water 5 minutes. Antigen retrieval was performed by boiling sections soaked in 10mM citrate buffer (pH 6.0) with microwave (500w) for 10 minutes. After boiling, sections were cooled down for 20 minutes on ice and blocked with blocking buffer (0.2% BSA and 0.1% Triton-X-100 in 1× D-PBS) for over 30 min. Then *t*he following procedures were same as the above.

For wholemount staining of isolated islets, fixed mouse islets were incubated in primary antibody in staining buffer (2% bovine serum albumin (A9647, Sigma-Aldrich) and 0.2% Triton-X100 (X100, Sigma-Aldrich) in 1× D-PBS) for at least 2 hours in room temperature. After wash with PBS, samples were incubated in secondary antibody diluted staining buffer for 2 hours. Samples were washed again and mounted with PBS.

RNA isolation and RT-PCR

Total RNA was isolated from islets according to the protocol supplied with RNeasy Mini Kit (74104, QIAGEN). Total RNA (1 μg) with 1 μl of oligo (dT), 1 μl of 10 mMdNTP Mix and distilled water in a final reaction volume of 28 μl mixture was heated to 65°C for 5 minutes and incubated on ice for at least 1 minute. This tube was added to the other tube containing 10 μl of 5X RT Buffer, 5 μl of 0.1 M DTT, 1 μl RNaseOUT™ Recombinant RNase Inhibitor (40 units/μl, Cat. no. 10777-019, Invitrogen Life Technologies) and 1 μl of SuperScript™ III RT (200 units/μl, Cat. no.18080093, Invitrogen Life Technologies) and heated to 50°C for 50 minutes and the reaction was inactivated by heating 85°C for 5 minutes.

Cloning of full length CAPS2

The cDNA sequence encoding the amino acid residues 90 through 1260 of the mouse CAPS2 isoform 7, was amplified by two polymerase chain reaction (PCR) using Phusion High-Fidelity DNA Polymerase (2 U/μL, Cat. no. F-530S, Invitrogen Life Technologies). Plasmid pCMV-3B was used as template. Amplification of CAPS2 (90-565) and CAPS2 (565-1260) uses two pair of oligonucleotide primers：

CAPS2-552-F-BamH1

(5′-CGGGATCCCTCTACGTCTTCGTGGTGAGG-3′) and

CAPS2-pcmv3b-mid-EcoR1-Rv

(5′-CTGTCTCTGGAGAATTCTGAAGAGGAAGGC-3′)；

CAPS2-pcmv3b-mid-EcoR1-Fw

(5′-GCCTTCCTCTTCAGAATTCTCCAGAGACAG-3′) and

CAPS2-PCMV3B-Xho1-Rv

(5′-CCTCTCGAGGAGCTGTGCATCATCAG -3′).

The underlined sequences primer sequences correspond, respectively, to the BamHI, EcoR1 and Xho1 restriction sites.

PCR was performed in a DNA Engine Peltier Thermal Cycler (BIO-RAD), and the program consisted of a single 98°C denaturation step for 1 min, followed by 35 cycles of denaturation at 98°C for 15 s, annealing at 60°C for 30 s and extension at 72°C for 2 min, followed by a final extension at 72°C for 5 min and ends at 4°C. The PCR

products were run on 1 % agarose gel and then purified using Gel/PCR DNA Fragments Extraction Kit (Cat. no. DF100, Geneaid).

The pCMV-myc-CAPS2wt (90-1260) was constructed in two steps that CAPS2 (565-1260) was cloned into pCMV-3B vector firstly and CAPS2 (90-565) was cloned into pCMV-3B inserted with CAPS2 (565-1260). The final PCR products of CAPS2 (90-565) and CAPS2 (565-1260) were digested with BamH1/EcoR1 and EcoR1/Xho1 enzymes respectively. The pCMV-3B vector was firstly digested with EcoR1/Xho1 and the digested CAPS2 (565-1260) was ligated into the vector using T4 ligase (Invitrogen). Then the recombinant plasmids were transformed into XL1 cells and the transformed bacteria were incubated on LB plates containing 50 μg/ml kanamycin at 37°C for 18 hr, and colonies containing the insert were identified by colony PCR. A positive clone for each construct was grown overnight in LB medium containing 50 μg/ml kanamycin, and then the plasmids were isolated using a Geneaid™ Mini Plasmid Kit (Cat. no. PAE40,Geneail) according to the manufacturer's protocol. After sequencing, pCMV-3B with CAPS2 (565-1260) insertion was used as template and digested by BamH1/EcoR1 enzymes. The digested CAPS2 (90-565) was subcloned into pCMV-myc-CAPS2 (565-1260) by the same procedures.

CAPS2 (1-90) was made from gene synthesis (Omics Bio) and subcloned into pCMV-myc-CAPS2 (90-1260) plasmid. The full-length pCMV-myc-CAPS2(1-1260)

was thus constructed.

Site direct mutagenesis of pCMV-myc-CAPS2(1-1260)

Single amino acid mutations of CAPS2 non-phosphorylatable mutation (T1016A, T1052A, T1231A) were created in pCMV-myc-CAPS2 (90-1260) using quick change site directed mutagenesis method. The mutagenic oligonucleotides (forward) used for T1016A, T1052A, T1231A are

Caps2-T1016A-F (5′-GTCAAAAGAACAAGAGCTGCGTTCGAACTC -3′), Caps2-T1052A-F (5′-CTAAAAAGCAAAGCGCCAAGCTGTGTGCC -3′), Caps2-T1231A-F (5′-CACAGACGTCTAGCTGTAGAGGAGGC -3′) respectively. For double amino acid mutations (T1016A+T1052A, T1052A+T1231A, T1016A+T1231A), caps2 T1016A or T1052A or T1231A was used as template to produce another mutagenic site. For triple amino acid mutations (T1016A+T1052A +T1231A), constructs of caps2 with double mutation sites was used as template. PCRs for single, double, triple amino acid mutations using PfuUltra II Fusion HS DNA Polymerase (Cat. no. 600670, Stratagene) were run for 2 min at 95°C, 18 cycles of 30 s at 95°C and 1 min at 55°C, followed by 4 min 30 s at 68°C. The resulting mutant plasmids were verified by DNA sequencing.

SIK2 constructs

The pCMV-flag-SIK2 wild-type (WT), kinase dead (KD), S587A mutant (non-PKA phosphorylatable mutant), S587D mutant (PKA phospho-mimicking mutant) were kindly provided by Dr. Sheng-Chung Lee (Institute of Molecular Medicine and Clinical Medicine, College of Medicine, National Taiwan University).

Transfection

For HEK 293T cell, transient transfection was performed with Lipofectamine^{TM} 2000 (Invitrogen, 11668-027) according to manufacturer's instructions.

For primary culture of islet cell, transient transfection was performed with Lipofectamine^{TM} 2000 (Invitrogen, 11668-027). In a 24-well format, cultured medium is replaced with 450 μl of Opti-MEM. 2.8 μl of Lipofectamine^{TM} 2000 are diluted in 25μl of Opti-MEM and incubated for 5 minutes then mixed with 0.5 μg of DNA diluted in 25μl of Opti-MEM. After 45 minutes of incubation, the 100 μl of mixed complexes are added to each well containing cultured islet cells and 450 μl of Opti-MEM. Cells are incubated at 37°C in a CO_2 incubator and Opti-MEM should be changed to normal culture medium after 5 hours.

Immunoprecipitation

Whole cell lysates from transfected HEK-293T cells were extracted by lysing cells with RIPA lysis buffer (20mM Tris/HCl, pH 7.4, 0.15M NaCl, 1mM DTT, 1mM EDTA, 1mM EGTA, 5% glycerol, 0.1% Triton X-100, 1X protease inhibitor (Roche) and 1X phosphatase inhibitor (Roche)) at 4°Cfor 15 min followed by centrifugation at 13000g, 4°Cfor 15 min .Immunoprecipitation was performed by incubating 500ug of protein from cell lysates with anti-Flag M2 magnetic beads (Sigma) at 4°C overnight. The precipitated proteins bound on M2 beads were washed 3 times with TBST (0.1% Tween 20 in 1× TBS) and added with 2X SDS sample buffer. Boiling at 95°C for 5 minutes afterwards dissociates the protein complex before western blot analysis.

In vitro kinase assay

The immunoprecipitated protein complexes were washed with TBST and kinase buffer (20 mMTris, pH 7.8, 10 mM $MgCl_2$, 50 mMNaCl, 1 mM DTT, 1 mM EGTA, protease inhibitor (Roche)). Kinase reaction was initiated by adding ATP 50 μM in 30 μl of kinase buffer then incubated the reaction mixture at 37°C for 30 min. Kinase reaction was terminated by adding 10 μl of 4X sample buffer and boiling at 95°C for 5

min. The level of p-Thr and other indicated proteins were analyzed by Western blot.

Western blot analysis

Proteins was separated by 6% SDS-PAGE and eletrophorestically transferred to polyvinylidenedifluoride (PVDF) membranes (PALL) at 300 mA for 2 hr. Membranes were probed with indicated primary antibody (CAPS2 1:200, Flag 1:200, C-Myc 1:200) at 4°C, overnight. After three times of washing by TBST (0.1% Tween 20 in 1× TBS), horseradish peroxidase-conjugated secondary antibodies were incubated for 2 hour at room temperature. Polypeptide bands were visualized using ECL chemiluminescent substrates (Advansta) and LAS-4000 luminescent image analyzer (Fujifilm).

Insulin ELISA

Insulin concentration was measured by using rat/mouse insulin ELISA kit (Mercodia). 10 μl of diluted samples were loaded into 96-microplate wells coated with antibodies. 100 μl of enzyme conjugate 1X solution was add into each well and incubate on a plate shaker (200 rpm) for 2 hr at room temperature. After incubation, samples in 96-microplate wells were wash with 350 μl of 1X wash buffer for six times. 200 μl of TMB substrate was added into each well and incubated for 15 min before 50 μl of stop

solution was added. Absorbance at OD 450 nm was detected by ELISA reader.

Results

The expression of SIK2 and CAPS2 in mouse pancreatic islets

In our work, we hypothesize that SIK2 regulates insulin secretion through the phosphorylation of CAPS2 in pancreatic β cells. Before studying the interaction between SIK2 and CAPS2, we want to check their expression in mouse pancreatic islets. The expression of SIK2 and CAPS2 proteins in islets of Langerhans was studied by immunohistochemistry of mouse pancreatic FFPE slides using SIK2, CAPS2 antibodies. Insulin antibody was used to mark the location of insulin producing β cells. Our data indicated that SIK2 and CAPS2 were both expressed in mouse pancreatic islets and located mainly in the insulin producing β cells (Figure 1).

Subcellular localization of SIK2 and CAPS2 in mouse pancreatic β cell

Although we can roughly study the expression of SIK2 and CAPS2 in islets from pancreatic FFPE slides, the subcellular localization such as insulin vesicles in β cells were limited to observe. Since the structure of islets of Langerhans is integrated and spheroid, it can be isolated and collected under microscope and each of the islet can directly be fixed and probed by antibodies without tissue processing. The wholemount immunofluorescent staining benefits us not only from time and effort saving, but let us

observe the original condition of intact islets freshly took out from the model animal (Figure 2). Additionally combined with the use of confocal microscope, subcellular localization of proteins in β cells was easily to be observed.

Thus we performed wholemount immunofluorescent staining on islets isolated from ICR mouse to go deep into the precise localization of SIK2 and CAPS2 in β cells. CAPS2 are cytosolic proteins that also peripherally associated with the membrane of large dense core vesicles (LDCV) in chromaffin cells [62]. Our data showed CAPS2 was expressed in the cytosol and formed vesicle-liked dots which were co-localized with insulin vesicles (Figure 3B). This result suggested in the case of β cells, CAPS2 was associated with insulin-containing LDCVs. However, SIK2 did not show vesicle-liked structures but diffusely expressed in the cytosol of β cells. Similarly, there were no enriched SIK2 signals found at CAPS2 vesicles (Figure 3A).

Cloning of β cells expressed CAPS2 isoform

There are 7 alternative splicing variants in mouse CAPS2 (CAPS2 v1~v7) (Reference to NCBI). CAPS2 v1, which lacks exon 25, represents the longest transcript and encodes the longest isoform. CAPS2 v2 is an isoform lacking exons 22 and 25, which encode part of the Munc13-1-homologous domain (MHD). CAPS2 v3 lacks

exons 11 and 22. CAPS2 v4, 5, 6 have C-terminal deletions from exon 14, exon 12, and exon 5, respectively. CAPS2 v7 lacks exons 17, 19 and 22 (Figure 4A). These isoforms can be subdivided into two groups: a long form containing the C-terminal MHD and a short form lacking the C-terminal MHD. CAPS2 v1, 2, 3 and 7 belong to the long-form group, while CAPS2 v4, 5 and 6 belong to the short-form group [63].

Different alternative splicing variants have distinct expression and functional properties. In order to investigate the role of CAPS2 and its interaction with SIK2 in pancreatic β cells, firstly we wanted to identify the β cells expressed CAPS2 splicing variants. As the MHD domain is involved in calcium dependent exocytosis and the C-terminal region is required for DCV (dense-core vesicle) binding, we target long-form group of CAPS2, which includes MHD domain and C-terminal region and may possess more complete functions. As a result, we designed primers by sequences of 5' end and 3' C-terminal region trying to clone it from isolated mouse pancreatic islets. The cDNA sequence encoding the mouse CAPS2 variant 7 was amplified and cloned into pCMV-3B vector (Figure 4B). The pCMV-CAPS2 v7-WT (wild-type) construct was transfected into HEK 293T cells to confirm if cells could correctly express the myc-tagged CAPS2 recombinant protein. Data from western blots showed HEK 293T cells could overexpress the exogenous myc-tagged CAPS2 recombinant protein probed by CAPS2 and myc antibodies and its molecular weight was larger than the endogenous

CAPS2 protein (Figure 4C). Also, immunofluorescent staining of HEK 293T cells transfected with this construct again confirmed the correct expression of exogenous myc-tagged CAPS2 recombinant protein in the cytosol (Figure 4D).

Physiological relevant proteins interaction between SIK2 and CAPS2

To study the correlation between SIK2 and CAPS2, we check their physiological relevant proteins interaction for a start by co-immunoprecipitation technique, a way using target protein-specific antibodies to indirectly capture proteins that are bound to a specific target protein. Furthermore, we wanted to experiment if their physiological relevant proteins interaction was in relation with SIK2's kinase activity. It has been reported that SIK2 suppressed CREB (cAMP-response element binging protein) mediated gene expression by phosphorylating its co-activator, TORC2. Nevertheless, cAMP-PKA dependent phosphorylation of SIK2 at Ser-587 diminished its TORC2 phosphorylation [42]. We therefore used SIK2-S587A mutant, the non-PKA phosphorylatable mutant, to mimic kinase active form and SIK2-S587D mutant, the PKA phosphorylating-mimicking mutant, to mimic kinase inactive form.

HEK 293T cells were co-transfected with pCMV-myc-CAPS2-WT construct as well as pCMV-flag-SIK2 constructs including Mock, SIK2-WT (wild-type),

SIK2-S587A (mimicked kinase active form), SIK2-S587D (mimicked kinase inactive form), SIK2-KD (kinase dead) respectively. Flag-SIK2 recombinant proteins were immunoprecipitated from the transfected HEK 293T cell lysates by a flag antibody and analyzed whether CAPS2 is its binging partner by western blot.

According to our data, CAPS2 was presented in the captured SIK2 protein complex and the amount of bound CAPS2 is associated with SIK2 kinase activity. CAPS2 proteins tended to bind SIK2 without kinase activity (SIK2-KD) active rather than wild-type SIK2 (SIK2-WT). In addition, the phosphorylation on SIK2 by PKA also affected its protein binding with CAPS2. However, both the non-PKA phosphorylatable mutantSIK2-S587A, thought as a SIK2 kinase active form,and the PKA phosphorylating-mimicking mutantSIK2-S587D, which mimics SIK2 kinase inactive form, showed increased levels on CAPS2 binding compared to wild-type SIK2 (SIK2-WT) (Figure 5) .

Putative SIK2 phosphorylation sites on CAPS2 and CAPS2-MUT-T1016A, T1052A, T1231A construct

After checking the physiological protein-protein interaction between SIK2 and CAPS2, we attempted to verify if CAPS2, the putative substrate of SIK2, would be

directly phosphorylated by SIK2. SIK2 is a serine/threonine kinase and its putative phosphorylation sites on CAPS2 predicted using by Scansite *in silico* database mining (http://scansite.mit.edu) were mostly on threonine residue. These putative target sites were scored and the lower the numbers were, the more optimal the target sites were. Threonine residues located at 1016, 1052, 1231 of CAPS2, which scored 0.00 could be the most potential SIK2 phosphorylation sites (Figure 6A). To further experiment whether SIK2 phosphorylates CAPS2 right on these 3 position, we made pCMV-myc-CAPS2-MUT (T1016A, T1052A, T1231A) construct by performing site direct mutagenesis via the replacement of threonine with alanine, which is the non-phosphorylatable mutation on pCMV-myc-CAPS2-WT construct at T1016, T1052, T1231 (Figure 6B).

***In vitro* phosphorylation of SIK2 on CAPS2**

We study enzymatic phosphorylation ability of SIK2 on CAPS2 by performing *in vitro* kinase assay, a method which puts a kinase and suspicious substrate together in a kinase reacting condition to see if the phosphorylation happens in vitro. HEK 293T cells were transfected with pCMV-myc-CAPS2-WT/MUT and pCMV-flag-SIK2-Mock/WT/S587A/S587D/KD constructs individually, and the expressed recombinant

proteins were captured form cell lysates by immunoprecipitation. CAPS2-WT and CAPS2-MUT proteins respectively were put together with SIK2 proteins owning different kinase activities for proceeding kinase reaction followed by western blot analysis. As the predicted SIK2 putative phosphorylation sites on CAPS2 were mostly on threonine residue, we used specific p-Thr antibody to detect p-Thr (phospho-threonine) level of CAPS2. Data revealed that SIK2 indeed phosphorylated CAPS2 at threonine residue. Since there was no signals from SIK2-KD, indicating the p-Thr signal of CAPS2 was truly came from SIK2 kinase activity. The p-Thr level of CPAS2-MUT (T1016A, T1052A, T1231A) was slightly decreased compared to CPAS2-WT, indicating that SIK2 would phosphorylate CAPS2 not only at T1016, T1052, T1231 but threonine at other position. Surprisingly, both the non-PKA phosphorylatable mutant SIK2-S587A and the PKA phosphorylating-mimicking mutant SIK2-S587D showed reduced kinase activity, suggesting SIK2-S587 is crucial for the regulation of SIK2 kinase activity. However there were not much differences in the CAPS2 phosphorylation level by SIK2-S587A or SIK2-S587D. (Figure 7).

Transfection and expression of pTimer-phogrin in primarily cultured islet cells

After verifying the interaction between SIK2 and CAPS2, we desired to reveal how

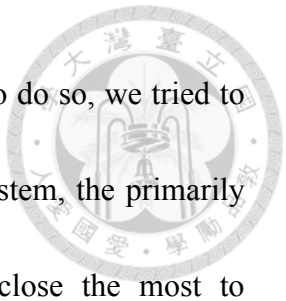

their cross-talk took part in insulin secretion in pancreatic β cells. To do so, we tried to conduct functional analysis of these two molecules in our model system, the primarily cultured β cells of isolated islets from ICR mice, which was close the most to physiological states instead of cell lines. These primary β cells attached to the bottom of culture dish and spread out after more than 3 weeks of culture. The capabilities of primary β cells to produce and secrete insulin were tested by immunofluorescent staining, suggesting primary β cells retained these abilities after long-term culture (Figure 8A).

We next tried to perform gene overexpression in primary β cells with lipofectamine transfection. Phogrin is a transmembrane protein expressed in pancreatic β cells, in which it is localized to the membrane of insulin-containing dense-core vesicles [64]. We delivered the pTimer-phogrin construct into primary β cells followed by immunocytochemistry targeting insulin. Results showed signals of pTimer-phogrin appeared to be granules which co-localized with most insulin vesicles, revealing transfection and expression with our procedures worked well in primarily cultured islet cells (Figure 8B).

Insulin secretion of SIK2/CAPS2 overexpressed mouse primary β cells

Followed by successful establishment of gene overexpression in primary β cells, we could begin to overexpress our purposed molecules and study their functions in β cells. Isolated pancreatic islets were collected and seeded separately under microscope into 24-well culture plate asa single islet seeded into each well. After a 3-week-culture, the attached islets were transfected with Mock, CAPS2, SIK2, and SIK2 plus CAPS2 constructs following the modified protocol for lipofectamine transfection. The next day after transfection, islets were starved for 30 min by the replacement with warmed HBSS before 16.7 mM of glucose stimulation. Solutions were collected at the beginning and at the end of starvation and every 15 min after glucose stimulation. The amounts of insulin secreted into solutions were measured by mouse insulin ELISA. In groups transfected with Mock, CAPS2, SIK2, and SIK2 plus CAPS2, we had 4, 2, 3 and 3 islets, respectively. In our system, there was a basal insulin secretion during 30 min of resting state. Upon glucose challenging, the amount of secreted insulin raised and reached the peak after 15 min. When islets transfected with CAPS2 or SIK2 alone, in which the balanced proportions between CAPS2 and SIK2 was interrupted, the basal insulin secretion was lower than islets transfected with mock (control group); however, the abilities to respond to glucose still remained, indicating CAPS2 and SIK2 were involved in basal insulin secretion. When islets transfected simultaneously with both SIK2 and CAPS2,inwhich the balance between CAPS2 and SIK2 maintained, the basal insulin

secretion was a bit restored. Furthermore, the glucose stimulated insulin secretion (from 0 to 15 min) was increased compared to control group. These results indicated SIK2, as a regulator, regulated insulin secretion via CAPS2, as an effecter, by sensitizing the responses to glucose of β cells.

Conclusion and Discussion

In this study, we provided evidences that CAPS2 was the downstream substrate of SIK2. On one hand, from the physiological protein interaction between SIK2 and CAPS2, we found CAPS2 was prone to associate with SIK2 without kinase activity (SIK2-KD) instead of the kinase-active SIK2 (SIK2-WT), suggesting the affinity between SIK2 and CAPS2 was lowered after the phosphorylation of CAPS2 by SIK2. This result may be due to the conformational change of CAPS2 after getting phosphorylated. In other words, SIK2 tends to bind with unphosphorylated CAPS2. On the other hand, our results from *in vitro* kinase assay demonstrated SIK2 indeed phosphorylates CAPS2 at threonine residue. Additionally, it has been reported that cAMP-PKA dependent phosphorylation of SIK2 at Ser-587 diminished phosphorylation of TORC2 by SIK2, which suppressed CREB (cAMP-response element binging protein) mediated gene expression. Our previous data indicated that SIK2 was phosphorylated by PKA on Ser587 upon glucose stimulation, which promoted insulin secretion. Equivalently, inhibition of SIK2 kinase activity by treating with selectively SIK2 kinase inhibitor (0.3 μM Compound C) increased insulin secretion. We thus assumed SIK2-S587 as kinase inactive form because it promoted insulin secretion. However, we discovered both non-PKA phosphorylatable SIK2-S587A mutant, which mimics SIK2 kinase active form, and PKA-phosphomimicking SIK2-S587D mutant, which mimics

SIK2 kinase inactive form, compromised SIK2 kinase activity compared to SIK2-WT. These results suggested SIK2-S587 is crucial for the regulation of SIK2 kinase activity as different substitutions at this position may result in the conformational changes and thus reduced its kinase function, which explained why SIK2-S587A and SIK2-S587D showed increased levels of SIK2-CAPS2 binging. That is to say, when kinase activity of SIK2 is restrained, it favors the formation of the SIK2-CAPS2 complex.

We performed gene overexpression in primarily cultured β cells to study how SIK2/CAPS2 crosstalk participates in insulin secretion. β cells co-expressed with both SIK2 and CAPS2, in which more SIK2-CAPS2 complexes may form, have strengthened responses to glucose stimulation (0~15 min). SIK2-CAPS2 complexes sensitize the rapid glucose stimulated insulin release possibly because it triggers the release of docked insulin vesicles.

Altogether, based on our results, we proposed a model (Figure 10) to elaborate how SIK2 regulates insulin secretion through binding with and phosphorylating on CAPS2. In basal state, SIK2 phosphorylates CAPS2 thereby interfere the binding between SIK2 and CAPS2. Upon glucose stimulation, the increased SIK2-S587 which was phosphorylated by cAMP dependent PKA pathway diminished its kinase activity therefore more SIK2-CAPS2 complexes could be composed. Consequently, releasing of docked insulin vesicles are promoted. Other possibilities are emerged that there are

probably other molecules take part in modulating phosphorylation and de-phosphorylation dynamics of CAPS2.

Nevertheless, the three most potential SIK2 phosphorylation site predicted on CAPS2 at T1016, T1052 and T1231 are not necessary for SIK2 phosphorylation because replacement of T with non-phosphorylatable A showed little decrease in p-Thr level. There were also other predicted phosphorylation site with higher probabilities on the mouse β cells expressed CAPS2 such as T434, T571, T793, T828.

Since different splicing variants of a protein may present different expression pattern and distribution, we therefore cloned β cells expressed CAPS2 splicing variants from mouse isolated islets. Sadakata et al in 2007 reported the differential expression and functional properties of six splicing variants in mouse CAPS2 that CAPS2 v1 was expressed exclusively in the brain, and CAPS2 v2~6 were highly expressed in the brain, but also in some non-neural tissues. Moreover in the brain, all isoforms showed predominant expression patterns in the cerebellum. CAPS2 v1 showed an up-regulated expression pattern in the developing cerebellum, whereas CAPS2 v2~6 exhibited transiently peaked expression patterns. CAPS2 v3 which lack the PH domain is important for membrane association, showed slightly decreased BDNF-releasing activity. In our experiment, CAPS2 variant 7 (Reference to NCBI), which lacks exons 17, 19 and 22, and encode part of the Munc13-1-homologous domain (MHD), was

identified in mouse pancreatic β cells. However, the expression, distribution and function of mouse CAPS2 variant 7 has yet been documented. The particular function of CAPS2 variant 7 and its interaction with SIK2 in pancreatic β cells are required more investigation.

CAPS1 and CAPS2 have been shown to regulate Ca^{2+}-dependent exocytosis of dense-core vesicle release of transmitters and hormones in neuroendocrine cells, but their precise roles in the secretory process still remain elusive. Speidel et al in 2007 pointed out the essential role of CAPS1 and CAPS2 in pancreatic β cells by generating $CAPS2^{-/-}$, and $CAPS1^{+/-}$; $CAPS2^{-/-}$mice, presenting glucose intolerance which is attributable to a marked reduction of glucose-induced insulin secretion. This phenomenon correlates with diminished Ca^{2+}-dependent exocytosis, a reduction in the size of the morphologically docked pool, and a decrease in the readily releasable pool of secretory vesicles. Accordingly, our proposed SIK2/CAPS2 model may support this study that knockout of CAPS2 cause inability to form SIK2-CAPS2 complexes contributed to the decreasing glucose stimulated insulin secretion.

For treatment of type 2 diabetes clinically, metformin and thiazolidinediones (TZDs), examples of the widely used drug decrease glucose production from liver and increase glucose utilization by skeletal myocyte, through the indirect activation of AMPK. AMPK is an energy-sensing enzyme that is activated when cellular energy

levels are low, and it signals to stimulate glucose uptake in skeletal muscles, fatty acid oxidation in adipose (and other) tissues, and reduces hepatic glucose production. AMPK activation improves insulin sensitivity and glucose homeostasis, making it an attractive target for T2D and metabolic syndrome. On the other side, insulin signaling pathways in peripheral tissues become defective under the circumstances of insulin resistance; as a result, the need for insulin is further enhanced. Increasing insulin secretion in order to compensate for insulin resistance is also essential way for treatment of type 2 diabetes. Our results here show that the cross talk between SIK2 and CAPS2 in β cells regulates insulin secretion responsed to glucose stimulation. Further study to reveal the molecular machineries of their interaction can potentially be applicable to develop novel medical strategies to confer symptoms of patients with type 2 diabetes.

References

1. Mehlen, P. and A. Puisieux, *Metastasis: a question of life or death.* Nat Rev Cancer, 2006. **6**(6): p. 449-58.
2. Stewart, B.W., et al., *World cancer report 2014*. xiv, 630 pages.
3. Jemal, A., et al., *Cancer statistics, 2004.* CA Cancer J Clin, 2004. **54**(1): p. 8-29.
4. Mazzone, P., et al., *Bronchoscopy and needle biopsy techniques for diagnosis and staging of lung cancer.* Clin Chest Med, 2002. **23**(1): p. 137-58, ix.
5. Velve-Casquillas, G., et al., *Microfluidic tools for cell biological research.* Nano Today, 2010. **5**(1): p. 28-47.
6. Velve Casquillas, G., et al., *Fast microfluidic temperature control for high resolution live cell imaging.* Lab Chip, 2011. **11**(3): p. 484-9.
7. Velve-Casquillas, G., et al., *A fast microfluidic temperature control device for studying microtubule dynamics in fission yeast.* Methods Cell Biol, 2010. **97**: p. 185-201.
8. Forry, S.P. and L.E. Locascio, *On-chip CO2 control for microfluidic cell culture.* Lab Chip, 2011. **11**(23): p. 4041-6.
9. Lu, P., V.M. Weaver, and Z. Werb, *The extracellular matrix: a dynamic niche in cancer progression.* J Cell Biol, 2012. **196**(4): p. 395-406.
10. Cox, T.R. and J.T. Erler, *Remodeling and homeostasis of the extracellular matrix: implications for fibrotic diseases and cancer.* Dis Model Mech, 2011. **4**(2): p. 165-78.
11. Jia, D., et al., *Development of a highly metastatic model that reveals a crucial role of fibronectin in lung cancer cell migration and invasion.* BMC Cancer, 2010. **10**: p. 364.
12. Sun, X., et al., *The EDA-containing cellular fibronectin induces epithelial-mesenchymal transition in lung cancer cells through integrin alpha9beta1-mediated activation of PI3-K/AKT and Erk1/2.* Carcinogenesis, 2014. **35**(1): p. 184-91.
13. Quail, D.F. and J.A. Joyce, *Microenvironmental regulation of tumor progression and metastasis.* Nat Med, 2013. **19**(11): p. 1423-37.
14. Yeh, H.Y. and J.C. Lin, *Surface characterization and in vitro platelet compatibility study of surface sulfonated chitosan membrane with amino group protection-deprotection strategy.* J Biomater Sci Polym Ed, 2008. **19**(3): p. 291-310.
15. Chen, Y.H., et al., *Control of cell attachment on pH-responsive chitosan surface by precise adjustment of medium pH.* Biomaterials, 2012. **33**(5): p. 1336-42.
16. Chen, Y.H., et al., *Cell fractionation on pH-responsive chitosan surface.*

Biomaterials, 2013. **34**(4): p. 854-63.
17. Chu, Y.W., et al., *Selection of invasive and metastatic subpopulations from a human lung adenocarcinoma cell line.* Am J Respir Cell Mol Biol, 1997. **17**(3): p. 353-60.
18. American Diabetes, A., *Diagnosis and classification of diabetes mellitus.* Diabetes Care, 2011. **34 Suppl 1**: p. S62-9.
19. *Classification and diagnosis of diabetes mellitus and other categories of glucose intolerance. National Diabetes Data Group.* Diabetes, 1979. **28**(12): p. 1039-57.
20. Daneman, D., *Type 1 diabetes.* Lancet, 2006. **367**(9513): p. 847-58.
21. Butler, A.E., et al., *Beta-cell deficit and increased beta-cell apoptosis in humans with type 2 diabetes.* Diabetes, 2003. **52**(1): p. 102-10.
22. American Diabetes, A., *Standards of medical care in diabetes--2014.* Diabetes Care, 2014. **37 Suppl 1**: p. S14-80.
23. Krupp, M.A., et al., *Current medical diagnosis & treatment*. McGraw-Hill Companies: New York etc. ,. p. v.
24. *Diabetes care.* Med Econ, 2004. **81**(17): p. 14, 16.
25. Jiang, Y.D., et al., *Incidence and prevalence rates of diabetes mellitus in Taiwan: analysis of the 2000-2009 Nationwide Health Insurance database.* J Formos Med Assoc, 2012. **111**(11): p. 599-604.
26. Seino, S. and G.I. Bell, *Pancreatic beta cell in health and disease*. 2008, Tokyo: Springer. xv, 474 p.
27. Ma, L., et al., *Direct imaging shows that insulin granule exocytosis occurs by complete vesicle fusion.* Proc Natl Acad Sci U S A, 2004. **101**(25): p. 9266-71.
28. Ammala, C., et al., *Exocytosis elicited by action potentials and voltage-clamp calcium currents in individual mouse pancreatic B-cells.* J Physiol, 1993. **472**: p. 665-88.
29. Rorsman, P. and E. Renstrom, *Insulin granule dynamics in pancreatic beta cells.* Diabetologia, 2003. **46**(8): p. 1029-45.
30. Neher, E., *Vesicle pools and Ca2+ microdomains: new tools for understanding their roles in neurotransmitter release.* Neuron, 1998. **20**(3): p. 389-99.
31. Parsons, T.D., et al., *Docked granules, the exocytic burst, and the need for ATP hydrolysis in endocrine cells.* Neuron, 1995. **15**(5): p. 1085-96.
32. Gromada, J., et al., *CaM kinase II-dependent mobilization of secretory granules underlies acetylcholine-induced stimulation of exocytosis in mouse pancreatic B-cells.* J Physiol, 1999. **518 (Pt 3)**: p. 745-59.
33. Barg, S., et al., *Fast exocytosis with few Ca(2+) channels in insulin-secreting mouse pancreatic B cells.* Biophys J, 2001. **81**(6): p. 3308-23.
34. Rorsman, P., et al., *The Cell Physiology of Biphasic Insulin Secretion.* News

Physiol Sci, 2000. **15**: p. 72-77.
35. Olofsson, C.S., et al., *Fast insulin secretion reflects exocytosis of docked granules in mouse pancreatic B-cells.* Pflugers Arch, 2002. **444**(1-2): p. 43-51.
36. Cheng, K., S. Andrikopoulos, and J.E. Gunton, *First phase insulin secretion and type 2 diabetes.* Curr Mol Med, 2013. **13**(1): p. 126-39.
37. Seino, S., T. Shibasaki, and K. Minami, *Dynamics of insulin secretion and the clinical implications for obesity and diabetes.* J Clin Invest, 2011. **121**(6): p. 2118-25.
38. Wang, Z., et al., *Cloning of a novel kinase (SIK) of the SNF1/AMPK family from high salt diet-treated rat adrenal.* FEBS Lett, 1999. **453**(1-2): p. 135-9.
39. Horike, N., et al., *Adipose-specific expression, phosphorylation of Ser794 in insulin receptor substrate-1, and activation in diabetic animals of salt-inducible kinase-2.* J Biol Chem, 2003. **278**(20): p. 18440-7.
40. Lin, X., et al., *SIK (Salt-inducible kinase): regulation of ACTH-mediated steroidogenic gene expression and nuclear/cytosol redistribution.* Endocr Res, 2000. **26**(4): p. 995-1002.
41. Jhala, U.S., et al., *cAMP promotes pancreatic beta-cell survival via CREB-mediated induction of IRS2.* Genes Dev, 2003. **17**(13): p. 1575-80.
42. Screaton, R.A., et al., *The CREB coactivator TORC2 functions as a calcium- and cAMP-sensitive coincidence detector.* Cell, 2004. **119**(1): p. 61-74.
43. Muraoka, M., et al., *Involvement of SIK2/TORC2 signaling cascade in the regulation of insulin-induced PGC-1alpha and UCP-1 gene expression in brown adipocytes.* Am J Physiol Endocrinol Metab, 2009. **296**(6): p. E1430-9.
44. Park, J., et al., *SIK2 is critical in the regulation of lipid homeostasis and adipogenesis in vivo.* Diabetes, 2014. **63**(11): p. 3659-73.
45. Sasaki, T., et al., *SIK2 is a key regulator for neuronal survival after ischemia via TORC1-CREB.* Neuron, 2011. **69**(1): p. 106-19.
46. Horike, N., et al., *Downregulation of SIK2 expression promotes the melanogenic program in mice.* Pigment Cell Melanoma Res, 2010. **23**(6): p. 809-19.
47. Ahmed, A.A., et al., *SIK2 is a centrosome kinase required for bipolar mitotic spindle formation that provides a potential target for therapy in ovarian cancer.* Cancer Cell, 2010. **18**(2): p. 109-21.
48. Fu, A., C.E. Eberhard, and R.A. Screaton, *Role of AMPK in pancreatic beta cell function.* Mol Cell Endocrinol, 2013. **366**(2): p. 127-34.
49. Sakamaki, J., et al., *Role of the SIK2-p35-PJA2 complex in pancreatic beta-cell functional compensation.* Nat Cell Biol, 2014. **16**(3): p. 234-44.
50. Henriksson, E., et al., *The AMPK-related kinase SIK2 is regulated by cAMP via phosphorylation at Ser358 in adipocytes.* Biochem J, 2012. **444**(3): p. 503-14.

51. Speidel, D., et al., *CAPS1 regulates catecholamine loading of large dense-core vesicles.* Neuron, 2005. **46**(1): p. 75-88.
52. Cisternas, F.A., et al., *Cloning and characterization of human CADPS and CADPS2, new members of the Ca2+-dependent activator for secretion protein family.* Genomics, 2003. **81**(3): p. 279-91.
53. Khodthong, C., et al., *Munc13 homology domain-1 in CAPS/UNC31 mediates SNARE binding required for priming vesicle exocytosis.* Cell Metab, 2011. **14**(2): p. 254-63.
54. Nguyen Truong, C.Q., et al., *Secretory vesicle priming by CAPS is independent of its SNARE-binding MUN domain.* Cell Rep, 2014. **9**(3): p. 902-9.
55. Parsaud, L., et al., *Calcium-dependent activator protein for secretion 1 (CAPS1) binds to syntaxin-1 in a distinct mode from Munc13-1.* J Biol Chem, 2013. **288**(32): p. 23050-63.
56. Speidel, D., et al., *A family of Ca2+-dependent activator proteins for secretion: comparative analysis of structure, expression, localization, and function.* J Biol Chem, 2003. **278**(52): p. 52802-9.
57. Binda, A.V., N. Kabbani, and R. Levenson, *Regulation of dense core vesicle release from PC12 cells by interaction between the D2 dopamine receptor and calcium-dependent activator protein for secretion (CAPS).* Biochem Pharmacol, 2005. **69**(10): p. 1451-61.
58. Shinoda, Y., et al., *Calcium-dependent activator protein for secretion 2 (CAPS2) promotes BDNF secretion and is critical for the development of GABAergic interneuron network.* Proc Natl Acad Sci U S A, 2011. **108**(1): p. 373-8.
59. Sadakata, T., et al., *Autistic-like phenotypes in Cadps2-knockout mice and aberrant CADPS2 splicing in autistic patients.* J Clin Invest, 2007. **117**(4): p. 931-43.
60. Liu, Y., et al., *CAPS facilitates filling of the rapidly releasable pool of large dense-core vesicles.* J Neurosci, 2008. **28**(21): p. 5594-601.
61. Neuman, J.C., et al., *A method for mouse pancreatic islet isolation and intracellular cAMP determination.* J Vis Exp, 2014(88): p. e50374.
62. Berwin, B., E. Floor, and T.F. Martin, *CAPS (mammalian UNC-31) protein localizes to membranes involved in dense-core vesicle exocytosis.* Neuron, 1998. **21**(1): p. 137-45.
63. Sadakata, T., M. Washida, and T. Furuichi, *Alternative splicing variations in mouse CAPS2: differential expression and functional properties of splicing variants.* BMC Neurosci, 2007. **8**: p. 25.
64. Caromile, L.A., et al., *The neurosecretory vesicle protein phogrin functions as a phosphatidylinositol phosphatase to regulate insulin secretion.* J Biol Chem,

2010. **285**(14): p. 10487-96.

Figures

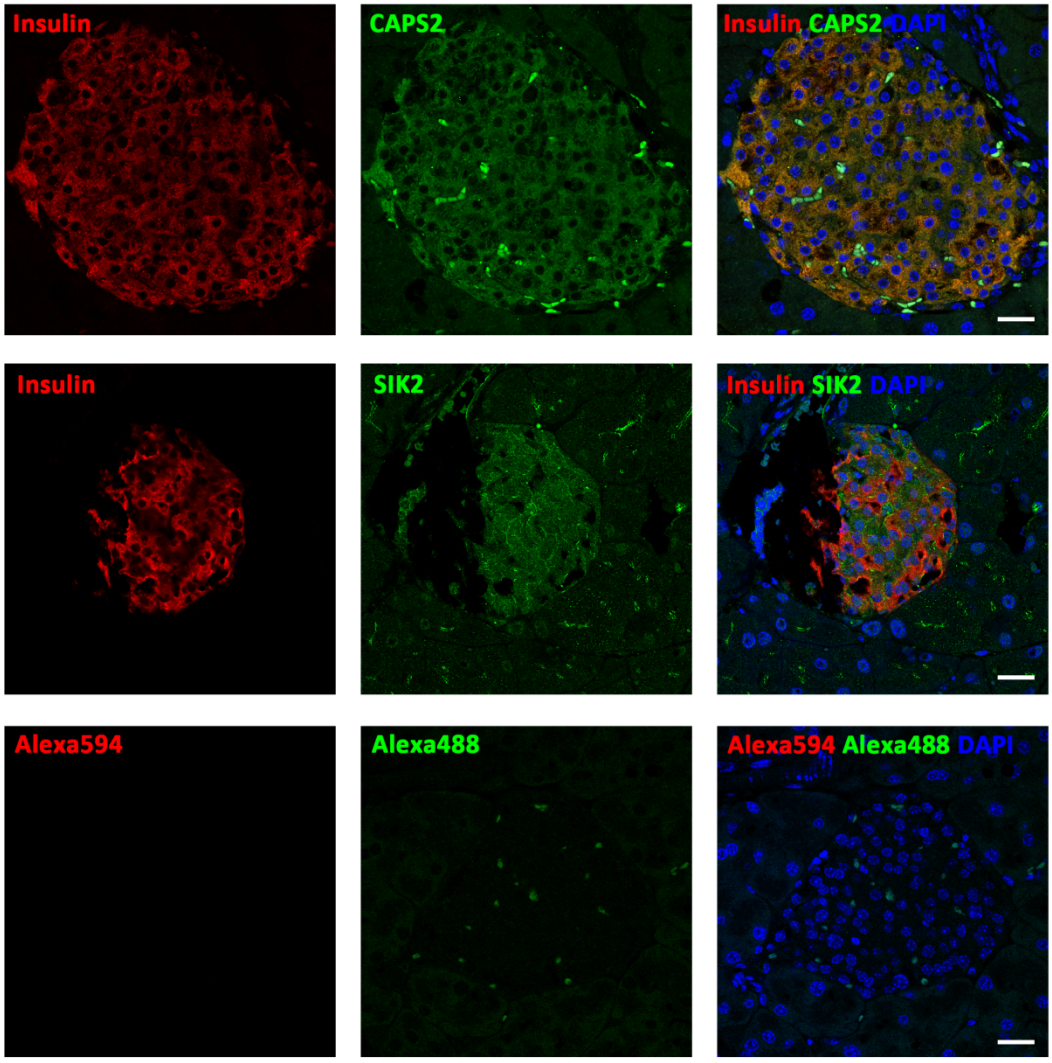

Figure 1. The expression SIK2 and CAPS2 in mouse pancreatic islets Immunohistochemistry of mouse pancreatic FFPE slides using SIK2, CAPS2, insulin antibodies. Alexa594 and Alexa488 secondary antibodies were used as negative control. Scale bar = 25 μm.

(A)

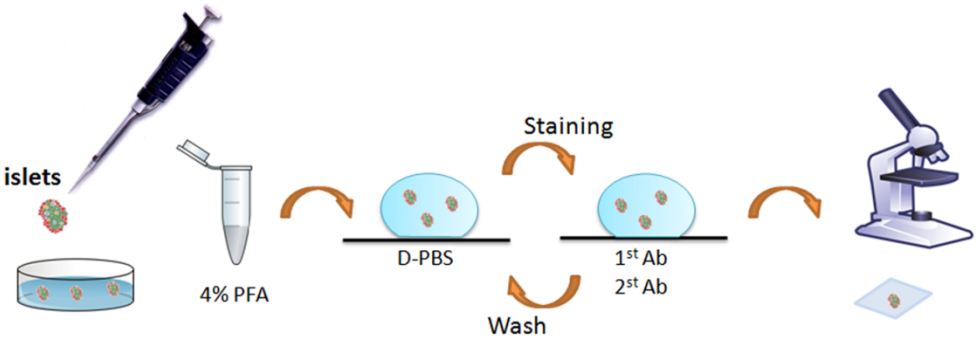

(B)

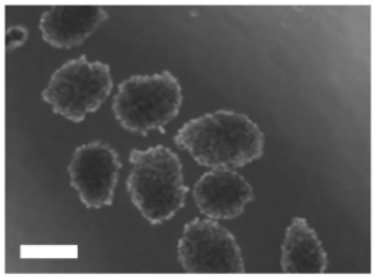

(C)

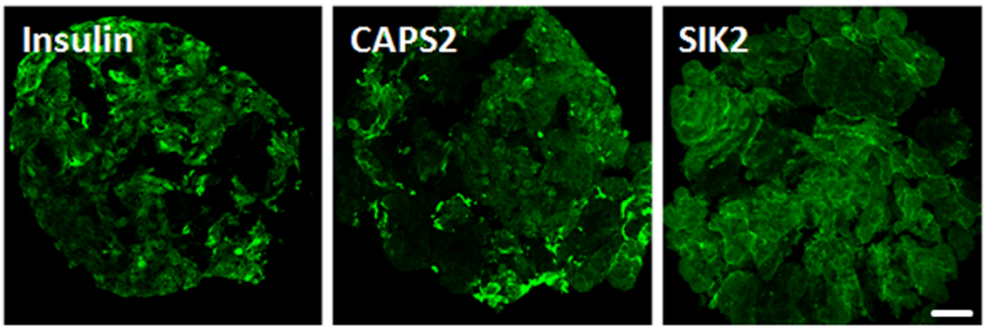

Figure 2. Wholemount immunofluorescent staining of isolated islets

(A) Schematic of wholemount immunofluorescent staining procedures on isolated islets from ICR mice. (B) Bright field image of freshly isolated mouse islets in PBS. Scale bar = 200 μm. (C) Wholemount immunofluorescent staining on isolated mouse islets with SIK2, CAPS2, insulin antibodies. Scale bar = 100 μm.

(A)

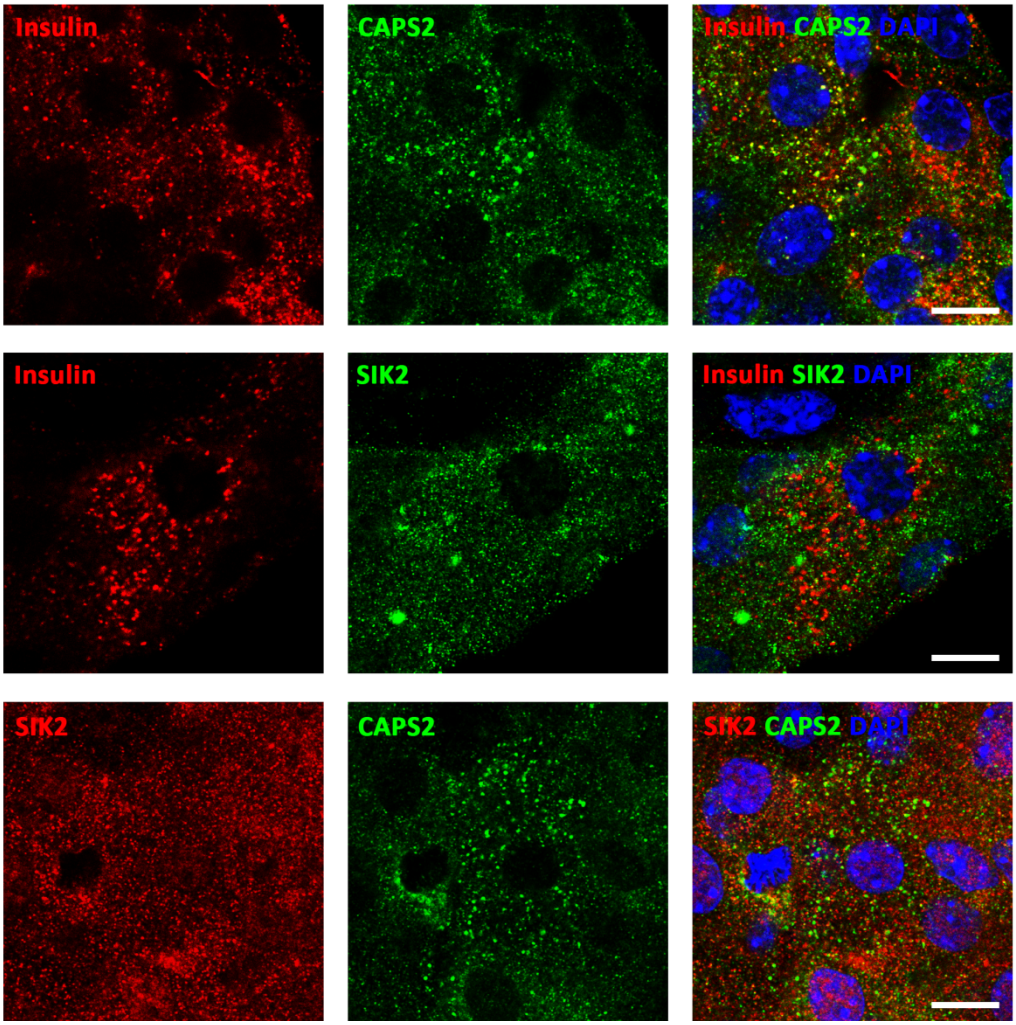

(B)

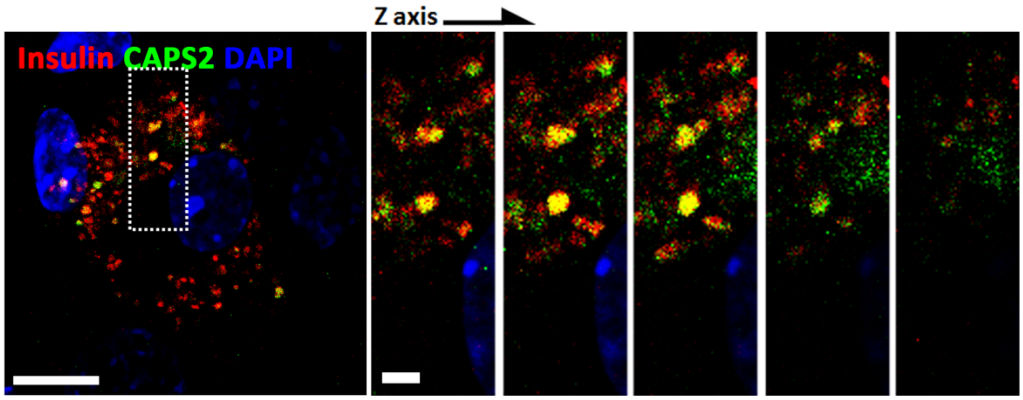

Figure 3. Subcellular localization of SIK2 and CAPS2 in mouse pancreatic β cell
(A)Wholemount immunofluorescent staining on isolated mouse islets with SIK2, CAPS2, insulin antibodies by confocal imaging. Scale bar = 10 μm. (B) Z stack images of immunofluorescent staining on mouse pancreatic β cell co-stained with insulin and

CAPS2. Image inside dotted frame showing the co-localization of CAPS2 and insulin vesicles was magnified and presented with serial Z positions. Images were collected at 0.3 μm intervals. Scale bar = 10 μm and 2 μm.

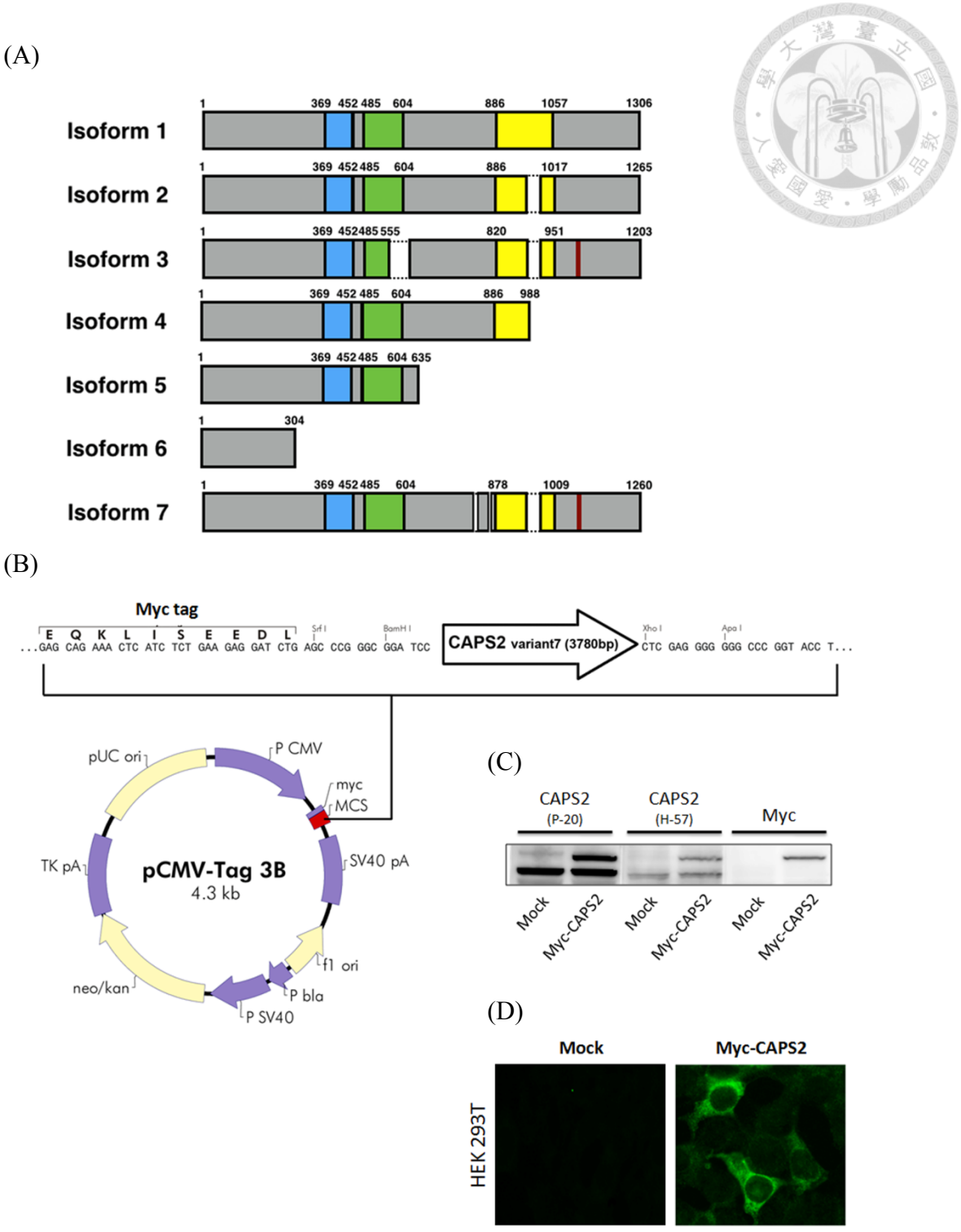

Figure 4. Cloning of CAPS2 from mouse pancreatic islets

(A) Domain structure of seven identified mouse CAPS2 isoforms. Blue, green and yellow boxes represent C2 domain, PH domain, MHD domain respectively. Numbers refer to the amino acids defining each domains and dotted lines refer to alternatively spliced exons. (B) Construct map of pCMV-CAPS2 v7-WT cloned from cDNA of isolated mouse pancreatic islets. (C) Western blot analysis of HEK 293T cells

transfected with pCMV-3B vector (mock) or pCMV-CAPS2 v7-WT construct. The endogenous CAPS2 protein and exogenous myc-tagged CAPS2 recombinant protein were probed by CAPS2 (P-20, H-57) and myc antibodies. (D) Immunofluorescent staining of HEK 293T cells transfected with pCMV-3B vector (mock) or pCMV-CAPS2 v7-WT construct. The exogenous myc-tagged CAPS2 recombinant proteins were expressed and probbed by myc antibodies.

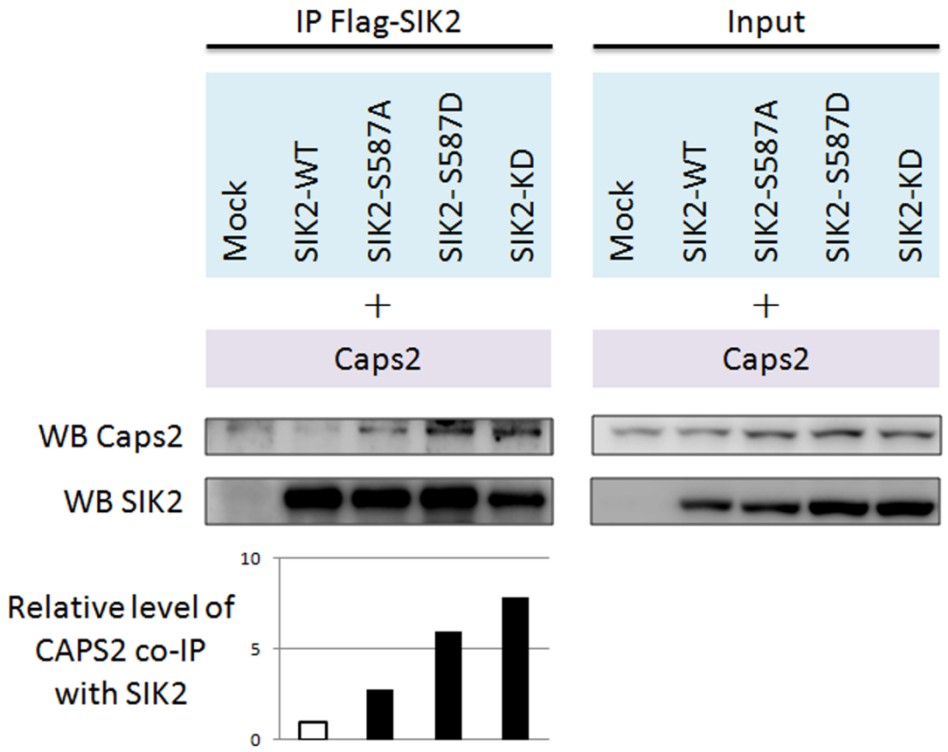

Figure 5. Physiological relevant proteins interaction between SIK2 and CAPS2

Co-immunoprecipitation of CAPS2 and SIK2 with different kinase activities. HEK 293T cells were co-transfected with pCMV-myc-CAPS2-WT construct as well as pCMV-flag-SIK2 constructs including Mock, SIK2-WT, SIK2-S587A, SIK2-S587D, SIK2- KD respectively. Flag-SIK2 recombinant proteins were immunoprecipitated by flag antibody and analyzed whether CAPS2 is its binging partner by western blot. A total of10%cell lysate was loaded in the input lanes.

(A)

SIK2 phosphorylation motif				
(Hy){(B)X or X(B)}XX(S/T)XXX(Hy)				
Species	**Protein**	**Motif**	**position**	**Score**
Mus	CAPS2	VKRTRTAFEL	1016	0.00
Mus	CAPS2	AKKQSTKLCA	1052	0.00
Mus	CAPS2	LHRRLTVEEA	1231	0.00
Mus	CAPS2	YVKLFTESTG	434	0.33
Mus	CAPS2	VKEGDTVIFA	571	0.33
Mus	CAPS2	MKDIATPIPA	793	0.33
Mus	CAPS2	AKIEETMNQA	828	0.33

(Positions with higher probability)

(B)

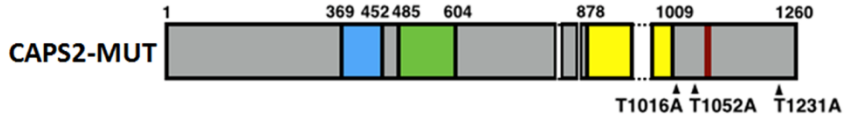

(C)

```
    WT 3315  GTCAAAAGAACAAGAACTGCGTTCGAACTC  3344
T1016A 3315  GTCAAAAGAACAAGAGCTGCGTTCGAACTC  3344

    WT 3424  CTAAAAAGCAAAGCACCAAGCTGTGTGCC  3452
T1052A 3424  CTAAAAAGCAAAGCGCCAAGCTGTGTGCC  3452

    WT 3963  CACAGACGTCTAACTGTAGAGGAGGC  3988
T1231A 3963  CACAGACGTCTAGCTGTAGAGGAGGC  3988
```

Figure 6. Putative SIK2 phosphorylation sites on CAPS2 and CAPS2-MUT-T1016A, T1052A, T1231A construct

(A) Putative SIK2 phosphorylation sites on mouse CAPS2 predicted by Scansite *in silico* database mining (http://scansite.mit.edu) using SIK2 phosphorylation consensus motif sequence as search reference. SIK2 phosphorylation consensus motif sequence is (Hy){(B)X or X(B)}XX(S/T)XXX(Hy) (Hy: hydrophobic amino acid, B: basic amino acid, S/T: serine or threonine, X: any amino acid, respectively). Color code for the conserved amino acid residues: hydrophobic residues G, A, V, I, L, M (blue), basic residues H, K, R (green), S or T residues (red) and any other amino acids (black). Threonine residues located at 1016, 1052, 1231 of mouse CAPS2 which scored 0.00 represents the most potential SIK2 phosphorylation sites. (B) Site direct mutagenesis of CAPS2 T1016, T1052, T1231 by the replacement of threonine with alanine. (C) Indicated primers for site direct mutagenesis.

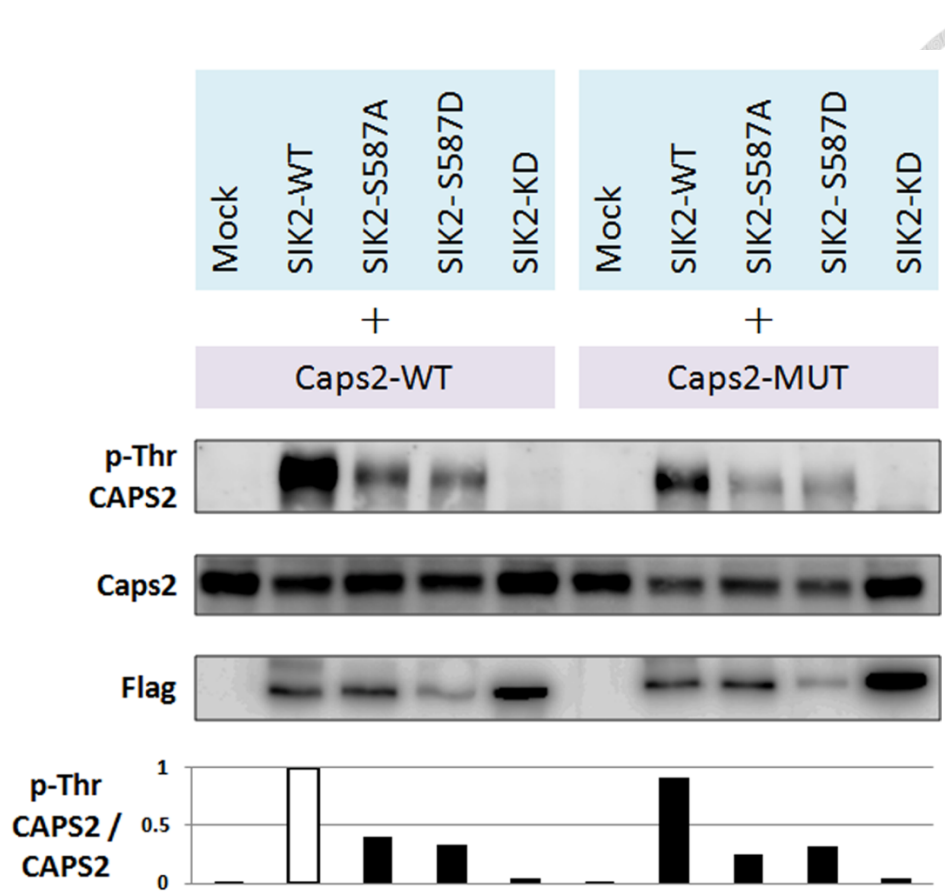

Figure 7. ***In vitro*** **phosphorylation of SIK2 on CAPS2**

In vitro kinase assay using immunoprecipitates of Flag-SIK2 (Mock, WT, S587A, S587D, KD) as kinases and Myc-CAPS2 (WT or MUT) as substrates. Phosphorylation of CAPS2 was detected by p-Thr (phospho-threonine) antibody. Phosphorylation level of CAPS2 by SIK2 was measured as p-Thr CPAS2 / total CPAS2.

(A)

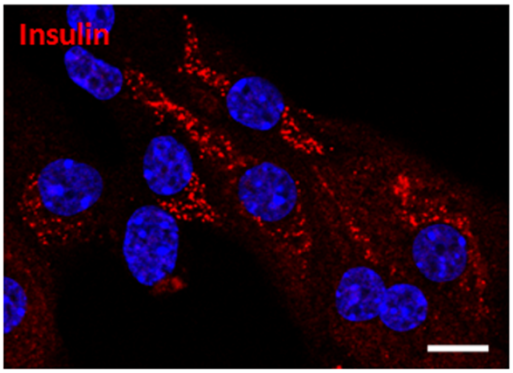

(B)

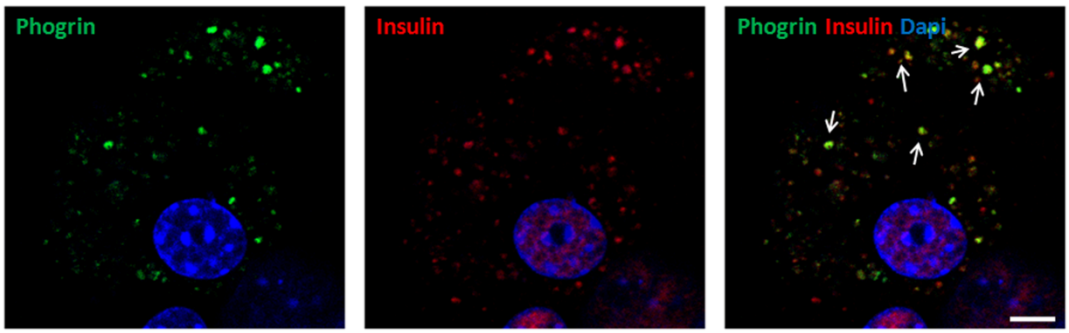

Figure 8. Transfection and expression of pTimer-phogrin in primarily cultured islet cells

(A) Immunofluorescent staining of primarily cultured β cells from isolated ICR mouse islets with insulin antibodies. Scale bar = 10 μm. (B) Images of primary β cells transfected with pTimer-phogrin and detected by 488 nm laser. Immunofluorescent staining with insulin antibodies showed phogrin was co-localized with insulin vesicles (white arrows). Scale bar = 5 μm.

(A)

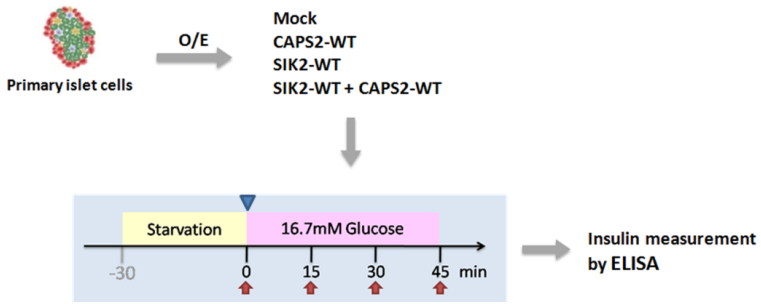
Primary islet cells
O/E
Mock
CAPS2-WT
SIK2-WT
SIK2-WT + CAPS2-WT
Starvation
16.7mM Glucose
-30
0
15
30
45 min
Insulin measurement
by ELISA

(B)

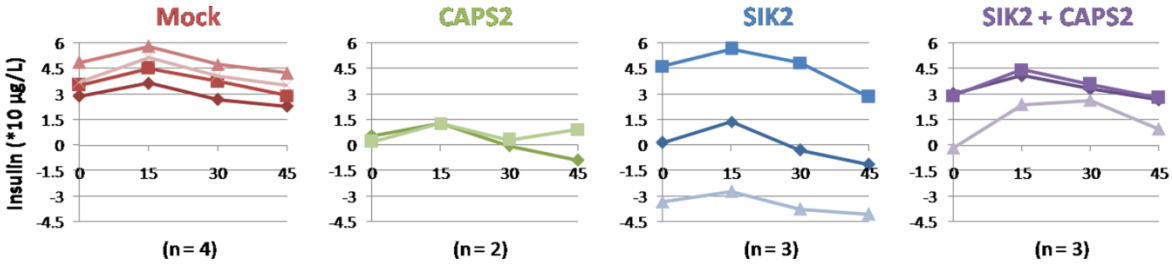
Mock
CAPS2
SIK2
SIK2 + CAPS2
Insulin (*10 μg/L)
(n = 4)
(n = 2)
(n = 3)
(n = 3)

(C)

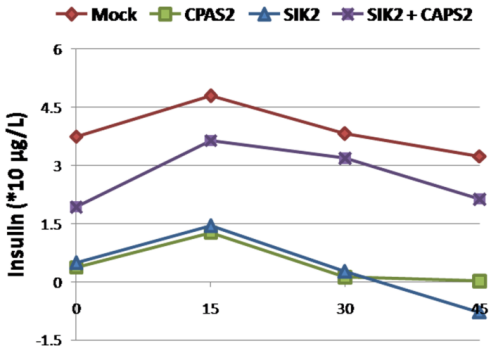
Mock
CPAS2
SIK2
SIK2 + CAPS2
Insulin (*10 μg/L)

(D)

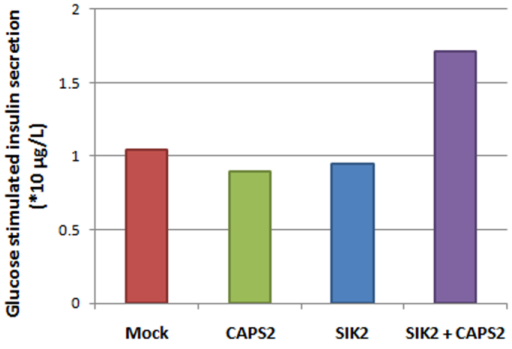
0~15 min
Glucose stimulated insulin secretion
(*10 μg/L)
Mock
CAPS2
SIK2
SIK2 + CAPS2

(E)

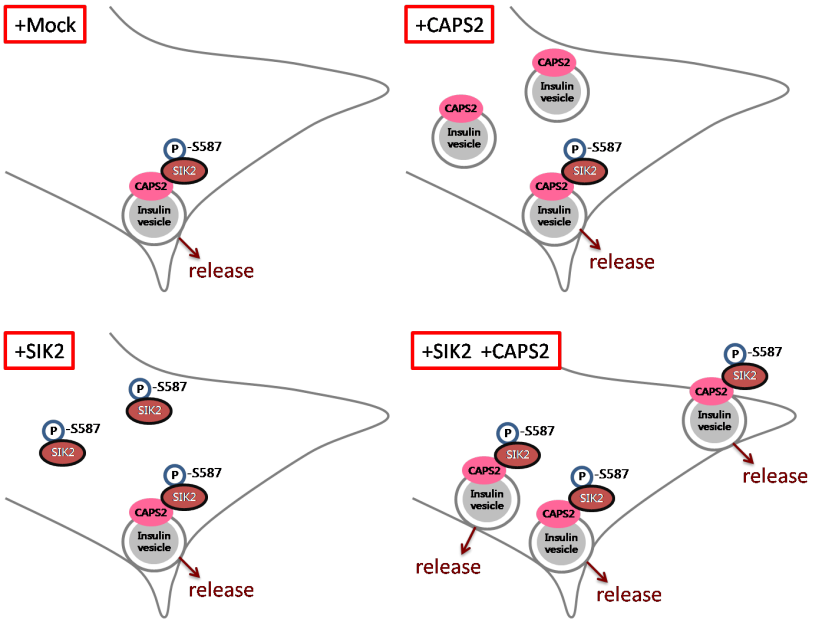
+Mock
+CAPS2
+SIK2
+SIK2 +CAPS2
P -S587
SIK2
CAPS2
Insulin vesicle
release

Figure 9. Insulin secretion of SIK2/CAPS2 overexpressed mouse primary β cells
(A) Schematic illustration of experimental design. Primarily cultured islets were transfected with Mock, CAPS2, SIK2, and SIK2 plus CAPS2 according to modified protocol. The next day after transfection, islets were starved for 30 min by the replacement with warmed HBSS before 16.7 mM of glucose stimulation. Solutions were collected at the beginning and at the end of starvation and every 15 min after glucose stimulation. Secreted insulin were measured by mouse insulin ELISA. (B) Respectively secreted insulin from islets transfected with Mock (n=4), CAPS2 (n=2), SIK2 (n=3), and SIK2 plus CAPS2 (n=3). (C) Average of secreted insulin from each group. (D) The glucose stimulated insulin secretion from 0 to 15 min. (E)The proposed model showing how SIK2 regulates insulin vesicle release upon glucose stimulation. Only if both SIK2 and CAPS2 are overexpressed, the amount SIK2/CAPS2 complexes increase. As the consequence, the rapid insulin release is promoted.

(A)

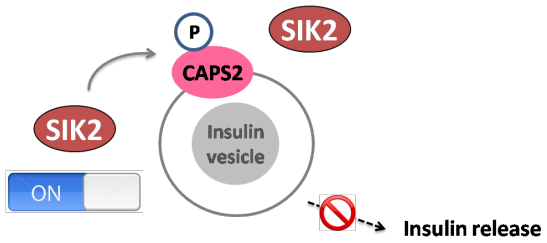

(B)

s

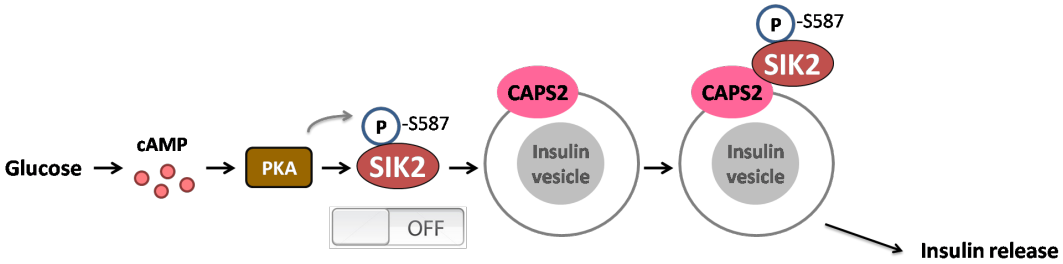

Figure 10. Proposed model of the SIK2/CAPS2 pathway

(A) Condition without glucose stimulation. SIK2 with active kinase activity would phosphorylate CAPS2, thereby interfere the binding between two proteins. (B) Condition with glucose stimulation. The cAMP-dependant PKA phosphorylation of SIK2-S587 inhibits its kinase activity. Unphosphorylated CAPS2 is able to form SIK2-CAPS2 complex which promotes insulin vesicle release.

Appendix

(A)

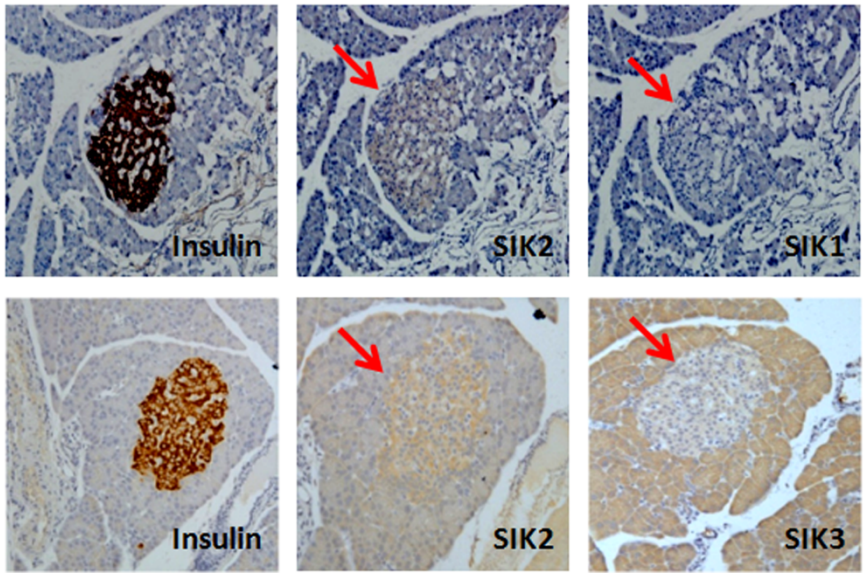

(B)

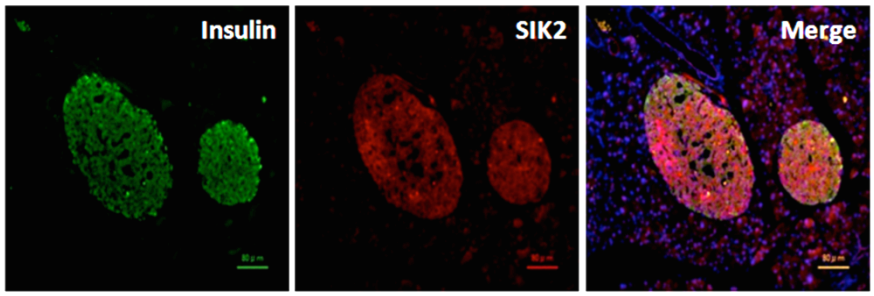

Appendix 1. Dominant expression of SIK2 rather than SIK1 or SIK3 in pancreatic islets mainly in insulin producing β cells

(A) Immunohistochemistry of FFPE pancreatic tissue slids from SD rat at 8 week of age with insulin, SIK1, SIK2 and SIK3 antibodies (red arrow). (B) Immunofluorescent staining of FFPE mouse pancreatic tissue slids with insulin and SIK2 antibodies.
(Data from Dr. Han-Yi Chou's lab: Pei-Han Tai)

(A)

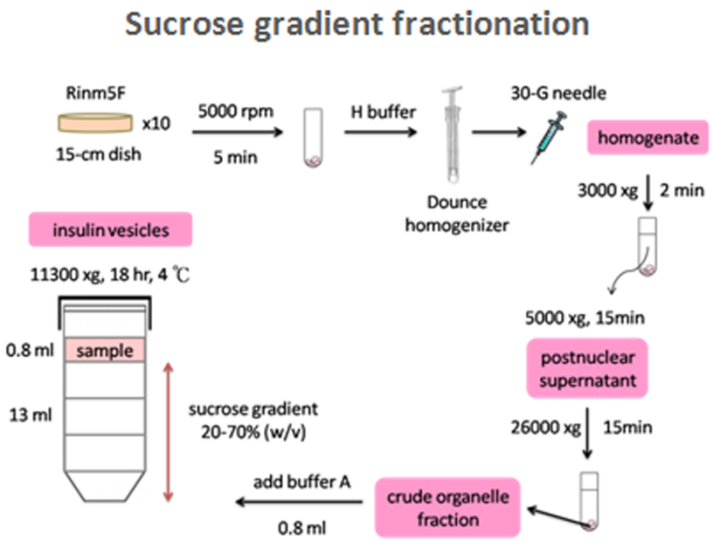

(B)

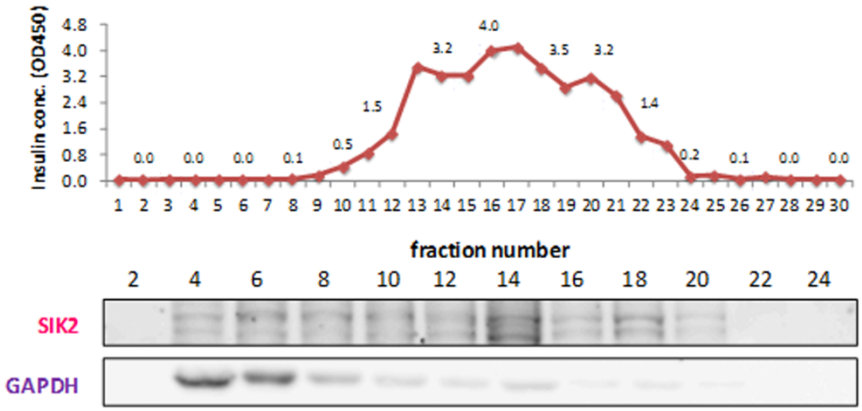

Appendix 2. Co-fractionation of SIK2 with insulin-containing LDCV in Rinm5F cells

(A) Schematic of biochemical sucrose gradient fractionation procedures of insulin vesicles form Rinm5F insulinoma cells (B) Insulin concentration of each fraction measured by insulin ELISA and fractionated samples precipitated with TCA (trichloroacetic acid) and analyzed by Western blot for the indicated proteins.

(Data from Dr. Han-Yi Chou's lab: I-I Chuo)

(A)

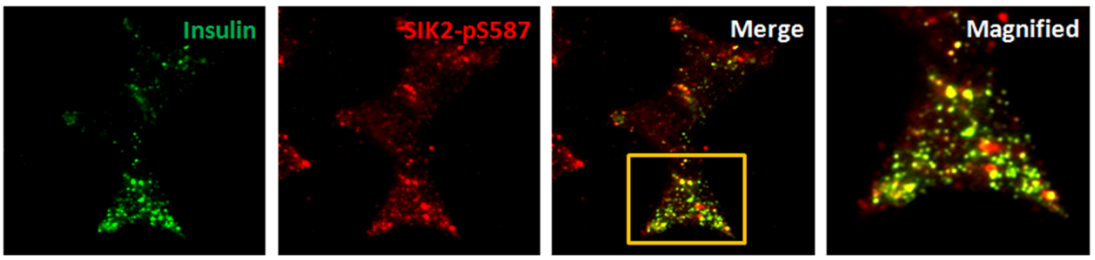

(B)

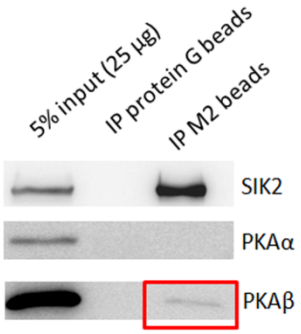

(C)

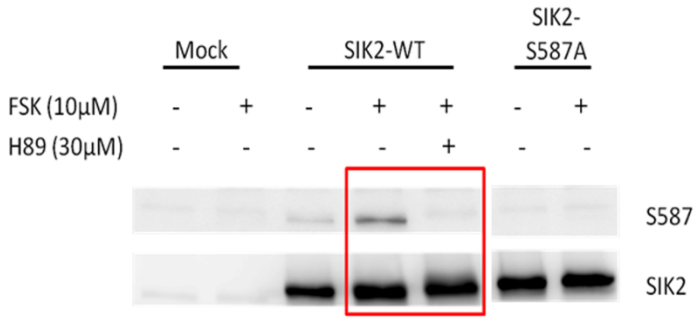

(D)

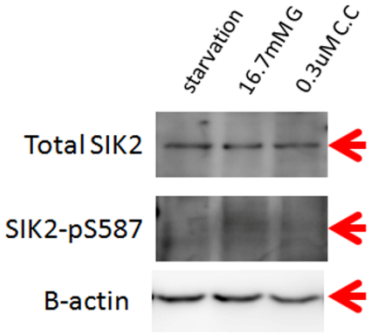

(E)

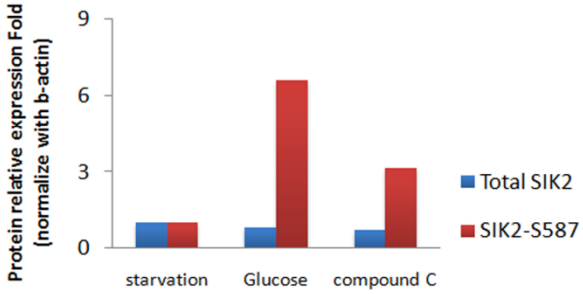

Appendix 3. Phosphorylation of SIK2-S587 by cAMP dependant PKA in β cells upon glucose stimulation (A) Immunofluorescent staining of RINm5F insulinoma cells with insulin and SIK2-S587 antibodies. SIK2-S587 was co-localized with insulin vesicles. (B) Co-immunoprecipitation of SIK2 and PKAβ. PKAβ instead of PKAα was presented in the same protein complex containing SIK2. (C) In vitro kinase assay of SIK2-WT and SIK2-S587A with the treatment of PKA activator (FSK) or PKA inhibitor. Phosphorylation level of SIK2-S587 was detected by SIK2-S587 and SIK2 antibodies. (D)(E) Western blot analysis of isolated mouse islets in starvation or treated with 16.7mM glucose or compound C (SIK2 inhibitor). SIK2 was phosphorylated at Ser587 under glucose or compound C treatments.

(Data from Dr. Han-Yi Chou's lab: Pei-Han Tai and Chung-Ju Kao)

(A)

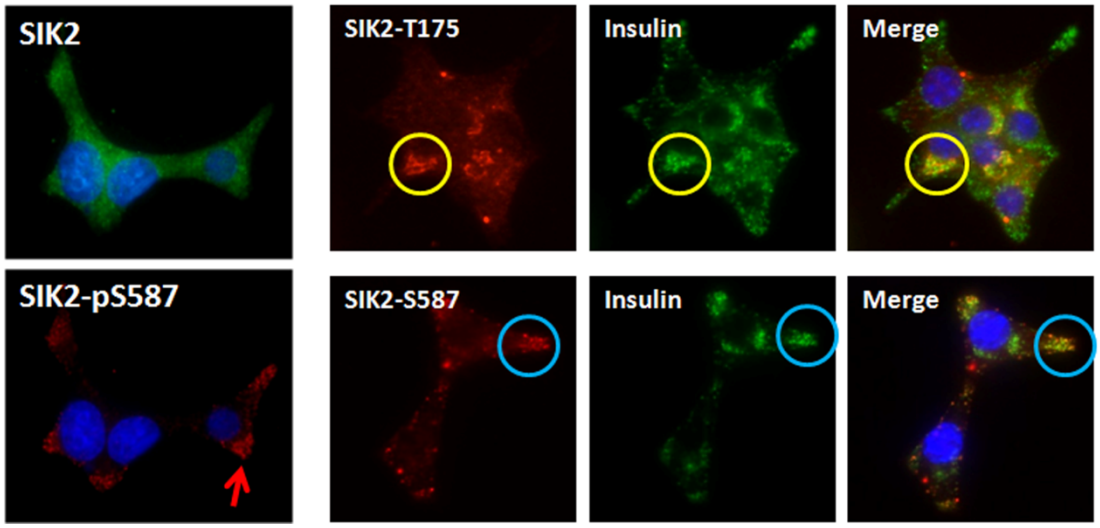

(B)

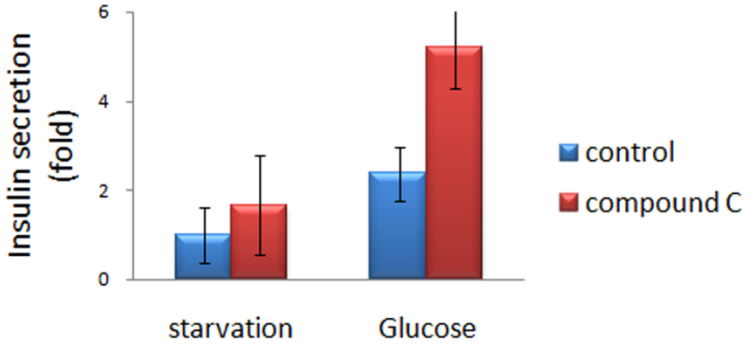

Appendix 4. Involvement of SIK2 kinase activity in insulin secretion

(A) Immunofluorescent staining of RINm5F cells with SIK2, SIK2-S587, SIK2-T175 and insulin antibodies. The kinase active SIK2-T175 and kinase inactive SIK2-S587 had distinct subcellular distribution that SIK2-T175 appeared in insulin vesicle around nuclear peripheral, while SIK2-S587 appeared in insulin vesicle near plasma membrane. (B) Secreted insulin measured by ELISA from RINm5F cells treated with Compound C (SIK2 inhibitor). Inhibition of SIK2 kinase activity by Compound C increased insulin secretion.

(A)

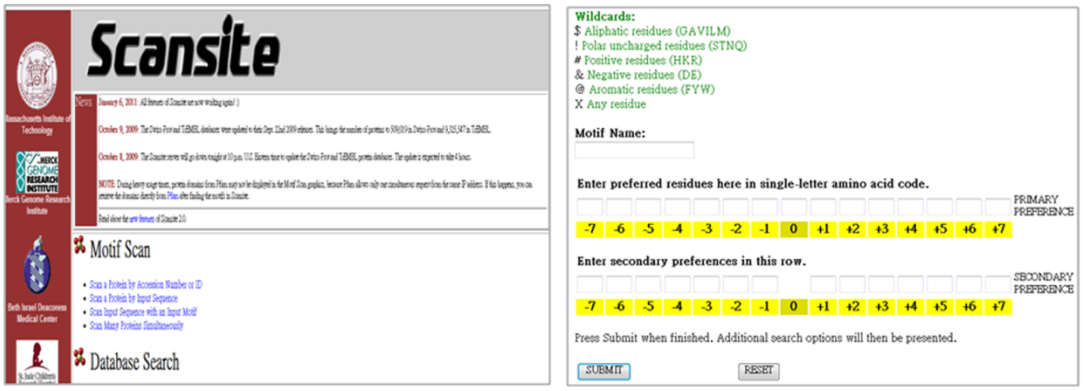

(B)

Canonical SIK2 phosphorylation motif (Hy)[(B)X or X(B)] XX(S/T)XXX(Hy)			
protein name	position	motif	score
Calcium-dependent secretion activator 2	1058	VKRTRTAFEL	0.00
	1094	AKKQSTKLCA	0.00
	1268	VHRRLTVEEA	0.00
Formin-binding protein 1	296	MKRTVSDNSL	0.00
	392	LKRGLSLKLG	0.00
Glutamate receptor-interacting protein 1	62	MKKEGTTLGL	0.00
	616	AHRTGTLELG	0.00
	983	GRKSVTLRKM	0.00
Coiled-coil domain-containing protein 2	73	AHRPVTQQGL	0.00
	580	IKKNVTKQIA	0.00
Voltage-gated K^+ channel subunit Kv7.1	199	ARKPISIIDL	0.00
	470	VRKSPTLLEV	0.00
Myoferlin	886	GRHKFSDVTG	0.00
	1174	LHRSKTTEII	0.00
Rho GTPase-activating protein 21	1741	MKKGKSTGSL	0.00
	1810	GHRDATEISV	0.00
Ras interaction/interference protein 3	92	VRRDSSSKQL	0.00
	572	VKKKPSMILG	0.00
Synaptotagmin-12	133	LRKSQSADSL	0.00
	413	LRRPVSMWHA	0.00
Serine/threonine-protein kinase TAO2	344	MHRAGTLTSL	0.00
	1082	VRRGISRLWL	0.00

Appendix 5. *In silico* search for putative SIK2 phosphorylation targets

(A) The Scansite motif search program at http://scansite.mit.edu developed by the Massachusetts Institute of Technology. (B) Putative SIK2 substrates containing multiple optimally match sites. The SIK2 phosphorylation consensus motif sequence (Hy){(B)X or X(B)}XX(S/T)XXX(Hy) (Hy: hydrophobic amino acid, B: basic amino acid, S/T: serine or threonine, X: any amino acid, respectively) was used as reference parameter.